Using water stable isotopes for tracing surface and groundwater flow systems in the Barlow-Ojibway Clay Belt, Quebec, Canada

SCHOLARONE™
Manuscripts

1   **Using water stable isotopes for tracing surface and groundwater flow**

2   **systems in the Barlow-Ojibway Clay Belt, Quebec, Canada**

3

4   Nathalie Rey[1*], Eric Rosa[1], Vincent Cloutier[1] and René Lefebvre[2]

5

6   [1] Groupe de Recherche sur l'Eau Souterraine, Institut de Recherche en Mines et en
7   Environnement, Université du Québec en Abitibi-Témiscamingue, Amos, Québec,
8   Canada, J9T 2L8.

9

10   *   Corresponding author: nathalie.rey@uqat.ca ((819) 732-8809 #8033)

11

12   [2] Centre Eau Terre Environnement, Institut national de la recherche scientifique,
13   Québec, Canada, G1K 9A9.

14

15

16

17

18

19   **Abstract**

20   This study aims to improve the understanding of surface and groundwater flow systems

21   based on water stable isotopes data in a 19,549 km^2 region of the Barlow-Ojibway Clay

22   Belt, in western Quebec, Canada. The available geochemical database contains

23   645 samples including precipitation, snow cores, surface waters, groundwater and

24   springs. All samples were analyzed for water stable isotopes (δ^2H-δ^{18}O) and

25   complementary tritium analyses were conducted on 98 groundwater and spring samples.

26   Precipitations depict a clear temperature-dependent seasonal pattern and define a local

27   meteoric water line (LMWL) without a latitudinal trend in δ^2H-δ^{18}O. Samples collected

28   from the snowpack plot on the LMWL, suggesting that the bulk snowpack preserves the

29   isotopic composition of precipitation throughout the frozen period, prior to the spring

30   snowmelt. Surface water samples define a local evaporation line (LEL) and evaporation

31   over inflow (E/I) ratios range between 0% and 36%. Groundwater and springs samples

32   are evenly distributed around the LMWL, suggesting that evaporation processes are

33   limited prior to infiltration and that surface waters do not significantly contribute to

34   groundwater recharge. Shallow unconfined aquifers present a greater variability in δ^2H-

35   δ^{18}O compared to confined aquifers located further down gradient, suggesting the mixing

36   of varied recharge waters along the regional groundwater flow system. A three-

37   component mixing model based on isotopic and specific electrical conductivity data

38   allows the quantification of such mixing processes. The interpretation of isotopic data

39   constrains a regional-scale conceptual model of groundwater flow systems and describes

40   processes related to the timing of recharge, evaporation, mixing and discharge.

41

42   **Keywords:**

43   Water stable isotopes; Groundwater; Surface waters; Precipitation; Boreal region

44

45   **Résumé**

46   Cette étude vise à mieux comprendre les systèmes d'écoulement dans une région de

47   19 549 km^2 au sein de la ceinture argileuse Barlow-Ojibway (ouest du Québec, Canada).

48   La base de données contient 645 échantillons analysés pour les isotopes stables de l'eau

49   (δ^2H-δ^{18}O) et inclue les précipitations, la neige au sol, les eaux de surface, les eaux

50   souterraines et les sources alors que 98 échantillons d'eau souterraine et de sources ont

51   été analysés pour l'activité tritium. La composition isotopique des précipitations présente

52   un cycle saisonnier dépendant de la température et définissant une droite locale des eaux

53   météoriques (DLEM) sans tendance δ^2H-δ^{18}O reliée à la latitude. Les données de neige

54   au sol tombent sur la DLEM, ce qui suggère que le couvert nival préserve sa composition

55   isotopique en hiver, avant la fonte des neiges printanières. Les échantillons d'eau de

56   surface définissent une droite évaporatoire locale (DEL) et les rapports de l'évaporation

57   sur les flux intrants variant entre 0% et 36% à l'échelle régionale. Les données d'eau

58   souterraine et de sources suggèrent que les processus d'évaporation sont limités avant

59   l'infiltration et que les eaux de surface contribuent peu à la recharge. Les aquifères à

60   nappe libre peu profonds présentent une plus grande variabilité isotopique par rapport aux

61   aquifères à nappe captive situés en aval le long des lignes d'écoulement, ce qui suggère

62   une atténuation de la variabilité isotopique issue de la recharge le long des systèmes

63   régionaux. Un bilan géochimique appuyé sur les données isotopiques et de conductivité

64   électrique de l'eau permet de quantifier ces mélanges. L'interprétation des données

65   isotopiques permet de contraindre des modèles conceptuels représentant les systèmes

66   d'écoulement régionaux et de documenter les processus de recharge, d'évaporation, de

67   mélange et de résurgence.

Introduction

68

69 Groundwater plays key functions for several ecosystems and represents an essential source of

70 potable water for approximately half of the world's population (Taylor et al. 2013). Nevertheless,

71 groundwater resources have been heavily used for human water supply and agriculture for many

72 years on a global scale (WWAP 2009) and climate change will most likely affect the hydrological

73 cycle and aquifers in the near future (Green et al. 2011). Groundwater resources are expected to be

74 increasingly stressed in response to demographic growth and growing water demand (Vörösmarty

75 et al. 2000). It is estimated that by 2025, nearly 50% of the world's population will be living in

76 water-stressed regions (WHO 2017). Such considerations stress the critical need to better

77 understand hydrogeological processes at various scales to support concrete actions aimed at

78 protecting groundwater resources, to maintain ecosystems and meet water supply needs of future

79 generations. Regionally and locally, groundwater protection must rely on land management

80 strategies that are based on an appropriate understanding of the hydrogeological system. This is

81 especially important in areas where most of the population relies on groundwater for potable water

82 supply, as is the case for the Abitibi-Temiscamingue region in western Quebec. This region is

83 renowned for its large eskers and moraines and for the remarkable quality of groundwater found

84 within the aquifers associated with these formations (Veillette et al. 2004; Collini et al. 2007).

85 However, these shallow unconfined aquifers are highly vulnerable to contamination and face

86 increasing human pressures such as forest operations, sand and gravel extraction, former in-trench

87 disposal sites, private and municipal wells and commercial water bottling (MRNF 2006; Nadeau et

88 al. 2015; Cloutier et al. 2016). The impacts on the groundwater resources associated with eskers

89 might also affect aquifers located down-gradient, further highlighting the need to better understand

90 regional hydrogeological processes. In this context, providing regional stakeholders with a coupled

91 understanding of physical and geochemical conditions is mandatory to ensure that land-use

92 decisions related to groundwater protection are based on reliable information.

93 Geochemical tracers are included in a wide spectrum of hydrological studies. They are increasingly

94 used to delineate flowpaths and quantify the processes affecting surface and groundwater resources

95 at various scales and in various regions of the world (e.g. Jeelani et al. 2013; Kortelainen and Karhu

96 2004; Wassenaar et al. 2011). Among the wide range of geochemical tracers that have been

97 exploited, water stable isotopes (^{2}H-^{18}O) data have provided unique insights into hydrological

98   processes (Araguás-Araguás et al. 2000; Gibson et al. 2005; Birks and Gibson 2009). The stable

99   isotopes of water are partitioned within a hydrological system, mainly in response to systematic

100 fractionation mechanisms occurring within the water cycle, including phase-change (solid-liquid-

101 vapour) processes, diffusion and rainout (Craig 1961; Rozanski et al. 1993; Gat 1996; Clark and

102 Fritz 1997). The isotopic composition of water is widely used in theoretical and applied

103 hydrological studies to document sources of atmospheric moisture and precipitation patterns

104 (Dansgaard 1964; Fritz at al. 1987), snow and ice-melting (Siegel and Mandle 1984), evaporation

105 processes in cold regions (Gat et al. 1994) and drylands (Kebede et al. 2009), sources mixing

106 (Ferguson et al. 2007; Wolfe et al. 2007) and groundwater recharge (Praamsma et al. 2009), among

107 other applications.

108 Cloutier et al. (2013; 2015; 2016) provided a comprehensive assessment of groundwater resources

109 in the Abitibi-Témiscamingue region, within the framework of the *Programme d'Acquisition de*

110 *Connaissances sur les Eaux Souterraines* (PACES) supported by the Quebec Ministry of the

111 Environment. A regional scale conceptual hydrogeological model representing regional flowpaths

112 from unconfined aquifers, located in recharge areas, to confined aquifers, found beneath the clay

113 belt, was proposed through the course of these studies. Nevertheless, the proposed conceptual

114 model is mainly constructed on the basis of physical hydrogeological data, whereas geochemical

115 data have not been yet fully exploited, which leads to important limitations in the understanding of

116 regional hydrogeological dynamics. Fitting into the pre-established framework, this study aims to

117 improve the understanding of regional surface and groundwater flow systems in the southern

118 portion of the Barlow-Ojibway Clay Belt (Abitibi-Témiscamingue, Quebec, Canada) on the basis

119 of geochemical data. The present study focuses on the stable (^{2}H-^{18}O) and radioactive (^{3}H) isotopes

120 of the water molecule. The proposed approach involves a regional-scale comprehensive assessment

121 of isotopic data within all hydrological components: precipitations, winter snowpack, surface

122 waters, groundwater and springs. The specific objectives of the present study are (1) to document

123 the atmospheric processes driving spatiotemporal variations in precipitation isotopic composition,

124 (2) to assess the potential interactions and mixing processes between surface waters and aquifers,

125 and (3) to decipher the mechanisms controlling the water isotopic variability in regional aquifers.

126 Ultimately, the data are interpreted to support an improved conceptual model of regional

127 groundwater flow systems representative of observed hydrogeological and geochemical conditions.

128

129 **Study Area**

130 The study area (Figure 1) covers 19,549 km^2 and corresponds to the municipalized territory of the

131 Abitibi-Temiscamingue region in Western Quebec, Canada. It encompasses the City of Rouyn-

132 Noranda and the Regional County Municipalities (RCM) of *La Vallée-de-l'Or*, *Abitibi*, *Abitibi-*

133 *Ouest* and *Témiscamingue*, for a total population of approximately 148,000 inhabitants (MAMROT

134 2016). It is estimated that more than 70% of this population relies on groundwater as a source of

135 domestic drinking water. The characteristics of the study area are briefly summarized below.

136 Further details about the hydrogeological framework can be found in Nadeau et al. (2015), Cloutier

137 et al. (2016), Nadeau et al. (2017) and within the geological maps of the Geological Survey of

138 Canada (Veillette 1986; 1987a; 1987b; Thibaudeau and Veillette 2005; Paradis 2005; 2007).

139

140 **Figure 1. Study area with the location of sampling sites**

141

142 *Physiography and hydrography*

143 The landscape of the study area is relatively flat, with elevations generally ranging

144 between 280 m and 320 m. The main positive reliefs correspond to heterogeneously

145 distributed bedrock outcrops, while the main depressions are associated with large lakes

146 (Abitibi, Témiscamingue and Simard; Figure 1). Despite its featureless landscape, the

147 region is crossed by the continental water divide separating surface waters of the

148 St. Lawrence River Basin (southern sector of the study area, Ottawa River watershed)

149 and those of the James Bay Basin (northern sector of the study area, Moose, Harricana

150 and Nottaway rivers watersheds).

151 *Climate and air masses*

152 The study region is characterized by a cold and humid continental climate with damp

153 summers, rather cold and long winters and a marked seasonality. The average monthly air

154 temperature remains below the freezing point from November to March (based on

155 Quebec Ministry of the Environment climate data; 1981-2010). The region is

156   characterized by a significant latitudinal thermal gradient and a difference of 2.1 °C

157   between the average annual air temperature in Temiscamingue (south) and Abitibi (north)

158   was reported by Asselin (1995). This difference is likely imparted by latitude and by the

159   influence of the continental water divide that creates a discontinuity between the northern

160   and southern sectors of the study area. The presence of numerous lakes on a territory

161   characterized by a gentle relief likely favors the development of buffered microclimates.

162   Such a phenomenon is documented in the vicinity of lakes Abitibi and Témiscamingue

163   (Asselin 1995). Cloutier et al. (2015) provided daily air temperatures and vertical inflows

164   based on interpolated data provided by *Centre d'Expertise Hydrique du Québec* (CEHQ)

165   for a period ranging from 1900 to 2010 (Poirier et al. 2012). Vertical inflows correspond

166   to the fluxes of water from liquid precipitations and from the melting of snow, and

167   therefore to the fluxes of water that are available for infiltration or surface runoff. If the

168   temperature is below the freezing point, vertical inflows can be null even if precipitation

169   events are observed. In the absence of snow on the ground and when precipitations fall as

170   liquid water, vertical inflows correspond to precipitation. Yearly average vertical inflows

171   range between 790.5 and 856.5 mm at the regional scale. The vertical inflows associated

172   with snow falling during the frozen period will mainly be observed during spring

173   snowmelt. The greatest vertical inflows are recorded in April for most of the study area,

174   except for the northernmost sector where maximum values are observed in May,

175   probably due to later thaw (Cloutier et al. 2015). Minimum vertical inflows are recorded

176   in January over the entire region due to temperatures that generally remain below the

177   freezing point. Regional-scale monthly averages of daily maximum and minimum

178   temperatures reveal that the warmest month is July (with daily average minimum and

179   maximum temperatures of 11.2 °C and 23.7 °C, respectively) and the coldest month is

180   January (with daily average minimum and maximum temperatures of -23.3 °C and -10.3

181   °C, respectively). The mean annual precipitation ranges from 875 mm for *La Vallée-de-*

182   *l'Or* RCM and 989 mm in the city of Rouyn-Noranda (Quebec Ministry of the

183   Environment climate data).

184   The main air masses affecting western Quebec are (1) the cold and dry Arctic, (2) the

185   moist and warm Maritime-tropical air that originates from the Caribbean, subtropical

186   Atlantic and Gulf of Mexico and migrates northwards following the Mississippi and

187   Missouri valleys before being deflected eastwards across the Great Lakes basin and (3)

188   the northern Pacific westerlies (Bryson 1966; Bryson and Hare 1974; Hare and Hay

189   1974). The Pacific westerlies are dominant in the continental climate for much of the year

190   (Hare and Hay 1974). Summers in the study area are warm and humid, reflecting the

191   dominance of Maritime-tropical air punctuated by intrusion of mild and dry westerlies.

192   Winters are influenced by Artic air masses that lead to cold and dry conditions (Bryson

193   and Hare 1974). The Abitibi-Temiscamingue region is characterized by weather

194   variability and instability reflecting the contribution of the different air masses. The

195   dominant winds generally originate from the northwest during winter and southwest

196   during summer. The polar jet stream, corresponding to the limit between the Arctic and

197   Maritime-tropical air masses, crosses the study area along a sinuous west-east pattern at

198   latitudes roughly corresponding to the position of the continental water divide.

199   *Hydrogeological framework*

200   The regional geological framework, as conceptually represented in Figure 2, is described

201   in details in numerous previous studies (Nadeau et al. 2015; Cloutier et al. 2016; Nadeau

202   et al. 2017; Veillette 1986; 1987a; 1987b; Veillette et al. 2004; Thibaudeau and Veillette 2005;

203   Paradis 2005; 2007) and it is thus only briefly presented here. Table 1 provides a summary

204   of the hydrological domains (atmosphere, surface, subsurface), components (precipitation

205   (snow, rain), surface water, groundwater, springs) and aquifers (granular (unconfined &

206   confined), fractured rock (unconfined & confined)) that are discussed in this study, in

207   relation with the main geological units of the region. The bedrock of the study area

208   (geological unit A in Figure 2) is composed of a wide variety of igneous, metamorphic

209   and metasedimentary rocks of the Abitibi and Pontiac sub-provinces, both components of

210   the Superior Geological Province. Groundwater flow within the bedrock is controlled by

211   the architecture of structural discontinuities. Cloutier et al. (2016) estimated hydraulic

212   conductivities ranging between 10^{-9} and 10^{-4} m/s for this unit. However, there is currently

213   no sufficient data to propose a regional-scale interpretation of bedrock hydrogeological

214   characteristics based on structural interpretations. Nevertheless, Rouleau et al. (1999)

215   proposed that groundwater flow within the bedrock of the study area is most likely

216   restricted to depths shallower than 75 m where sub-horizontal fractures are sufficiently

217   interconnected to allow significant groundwater flow. Most of the domestic wells of the

218   region are withdrawing groundwater from this unit using wells that are cased through

219   surficial sediments and open across the bedrock.

220

221   **Table 1. Summarized characteristics of the regional hydrogeological framework**

222

223   The oldest unconsolidated unit of the region corresponds to the till associated with the

224   last glaciation (geological unit B in Figure 2). It is recognized as a compact heterometric

225   geological unit characterized by a matrix composed of sand, silt and clay (Cloutier et al.

226   2015). The hydrogeological characteristics of this unit are poorly documented because it

227   is rarely exploited for groundwater supply, although it is not considered as a regional

228   aquitard (Cloutier et al., 2013; 2015). This till unit is overlain in places by glaciofluvial

229   sediments. The coarse grained glaciofluvial sediments (eskers and moraines; geological

230   unit C1 in Figure 2) of the region were mainly deposited at the emergence of subglacial

231   meltwater within proglacial Lake Barlow-Ojibway (Nadeau et al. 2015). These

232   formations are characterized by relatively high hydraulic conductivities, 10^{-6} to 10^{-1} m/s

233   according to Cloutier et al. (2016), and constitute the most productive unconfined

234   aquifers of the region (Nadeau et al. 2015). Other glaciofluvial sediments, mainly

235   consisting in finer sand and gravel, are also widespread between the main eskers and

236   moraines of the region (geological unit C2 in Figure 2). This unit is generally

237   characterized by hydraulic conductivities that are slightly lower than that of the eskers

238   and moraines (Cloutier et al. 2013; 2015; 2016). The glaciofluvial sediments are covered

239   in places by fine grained deep-water glaciolacustrine sediments deposited within

240   proglacial Lake Barlow-Ojibway (identified as the Clay Belt in Figure 1; geological unit

241   D in Figure 2). Owing to its structure consisting in centimeter-scale alternating layers of

242   clay and silt (varves), this unit is considered as a regional aquitard (Cloutier et al. 2015),

243   although silt horizons may allow preferential sub-horizontal groundwater flow.

244   Sublittoral sands and beach or eolian sediments (geological unit E in Figure 2) overlying

245   the fine grained deep-water glaciolacustrine sediments are spatially associated with the

246 glaciofluvial deposits whereas organic deposits (geological unit F in Figure 2) are
247 widespread across the region, with large peatlands often developing on the flanks of
248 eskers and moraines.

249 Given this geological framework, and based on previous work from Cloutier et al. (2016)
250 and Nadeau et al. (2017), four main types of aquifers are distinguished within the study
251 region (Figure 2) and used to regroup the isotopic data:

252 (1) **Unconfined granular aquifers**, mainly associated with glaciofluvial formations
253   (eskers and moraines; number 5 in Figure 2). These formations are characterized
254   by relatively high hydraulic conductivities and represent the most productive
255   aquifers of the region, providing a high quality resource to numerous municipal
256   and private wells.

257 (2) **Confined granular aquifers**, in sectors where till and glaciofluvial sediments are
258   covered by the fine grained deep-water glaciolacustrine sediments (number 6 in
259   Figure 2);

260 (3) **Unconfined fractured rock aquifers**, essentially restricted to sectors
261   characterized by bedrock and till outcrops (number 7 in Figure 2);

262 (4) **Confined fractured rock aquifers**, in sectors covered by fine grained deep-water
263   glaciolacustrine sediments (number 8 in Figure 2). Most residences in rural
264   sectors of the region withdraw water from private wells installed in this aquifer.

265 Cloutier et al. (2013; 2015; 2016) provided estimates of the average groundwater
266 recharge rates (GRR) by calculating the water balance for each parcel of the study region
267 on a monthly basis. The calculations were provided on a 100 m x 100 m grid over the
268 study region, using the following equation:

269 $GRR = VI - R - \Delta W_S - ET$ 　　　　　　　　　　　　　　　　　　Equation 1

270 These water balance calculations are based on the vertical inflows (VI) provided by
271 Poirier et al. (2012) and on hypotheses associated with the regional hydrogeological

272   framework for estimating runoff (R), water storage within the unsaturated soil (ΔW_S) and

273   evapotranspiration (ET). Runoff coefficients were estimated according to land use, soils

274   characteristics and surface slopes, among others. Potential evapotranspiration rates were

275   quantified using the Thornthwait (1944) equation with climate data from Poirier et

276   al. (2012). The water storage within the unsaturated zone and the available water for

277   transpiration were evaluated for the different soils based on estimates of water retention

278   capacities, wilting points and thickness of the root zone. The calculated recharge rates

279   range between less than 91 mm/yr in sectors where fine-grained deep-water

280   glaciolacustrine sediments are found and more than 300 mm/yr, mainly in sectors

281   corresponding to eskers / moraines and other unconfined granular aquifers. Overall,

282   maximum recharge rates are observed during the snowmelt period whereas the lowest

283   rates are recorded throughout the winter period, when temperatures are below the

284   freezing point.

285

286   **Figure 2. Regional hydrogeological conceptual model and water sampling scheme**

287   **used to characterize the isotopic signature of all hydrological system components**

288

289   **Methods**

290   *Sampling procedures and in situ measurements*

291   Overall, 645 water samples were analyzed for their isotopic composition (δ^2H-δ^{18}O) as

292   part of this study, over a period ranging from 2006 to 2015 (Figure 1; Table 2). Table 2

293   provides a summary of the available data and associated sampling periods. From this

294   dataset, 98 water samples (only springs and groundwater) were also analyzed for their

295   tritium (^{3}H) content, over a period ranging from 2006 to 2011. The procedures associated

296   with the sampling of precipitations, the snowpack, surface waters, springs and

297   groundwater are presented separately below.

298   **Table 2. Summary of available water stable isotope data**

Precipitation monitoring

Monthly composite precipitation samples were collected at four monitoring stations within the study area (Figure 1; Station 1 = Béarn; Station 2 = Montbeillard; Station 3 = Sainte-Hélène-de-Mancebourg; Station 4 = Amos). Samples were collected monthly from July 2013 to 2015 at stations 1-2-3 (Figure 1), three sites included in the Quebec Ministry of the Environment Climate Monitoring Network. Rainfall samples were collected using a 10.1 cm inside diameter *All Weather P-2000* standard rain gauges from *Productive Alternatives*. A thin layer (approximately 1 cm) of paraffin oil (Mineral Oil, Light (NF/FCC), *Fisher Chemical*) was added to the rain gages to prevent evaporation and plastic screens were installed at the base of the rain gauge funnels to block debris and insects. Snowfall samples were collected owing to the participation of local operators / observers associated with the monitoring network. These observers are mandated to make measurements of snow (calculated in terms of equivalent water) intercepted by shielded *Nipher* snow gauges. Snow samples are collected daily at stations 1 and 3 (but not at station 2 owing to logistical constraints), left to melt overnight and subsequently stored in 1 L high density polyethylene (HDPE) bottles. Daily samples are mixed in order to obtain composite monthly samples. Paraffin oil (Mineral Oil, Light (NF/FCC), *Fisher Chemical*) is added to the bottles in order to prevent evaporation. The Amos monitoring station (Station 4), in operation from September 2009 to 2015, is located on the roof of the university campus and is not associated with the MDDELCC climate network. At this station, rain and snow samples are collected daily using a 30 cm ID bucket. Snow samples were left to melt overnight at 4 °C and subsequently stored in HDPE bottles. Daily samples were combined to produce a monthly composite sample. In all cases, the volume of monthly composite samples was first evaluated in the laboratory and smaller aliquots were subsequently stored in 60 ml HDPE bottles and kept at 4 °C until stable isotopes (δ^2H-δ^{18}O) analyses.

Samples from the Snowpack

A sampling campaign was carried out in March 2014 in order to retrieve cores from the snowpack accumulated throughout the winter. Sampling sites were selected in the

328   western part of the study region in an effort to collect data in the vicinity of the grid

329   points used by the CEHQ for calculating vertical inflows (Poirier et al. 2012). At each

330   site, a straight trench varying in length from 5 m to 6 m was first dug in a direction

331   oriented perpendicular to the wind. Snow cores (n ≥ 5) were subsequently sampled at

332   ≤ 1 m intervals, on the side of the trench facing the dominant wind. Snow cores were

333   collected using 4.2 cm ID x 1.6 m length HDPE tubes allowing the collection of the

334   snowpack over its entire height. Samples were weighed on site using a *Mettler Toledo*

335   digital scale with a precision of 0.0001 kg in order to calculate equivalent water contents.

336   For each site, the collected snow cores were transferred and combined within wide neck

337   HDPE bottles in order to obtain > 800 g composite samples. Samples were kept frozen

338   within the tightly sealed wide neck bottles during the field campaign and subsequently

339   left to melt overnight at room temperature. The melted samples were filtered using

340   0.45 μm *Waterra FHT* cartridges to remove soil particles and/or windblown debris

341   embedded in the snow. The filtered samples were transferred into 30-60 ml HDPE

342   containers and stored at 4 °C until stable isotopes (δ^2H-δ^{18}O) analyses.

343

344   *Surface waters*

345   Surface water samples were collected in July 2009 and from July to October, 2013.

346   Rivers and streams were sampled near the central part of the main channel, at depths of

347   0.5-1.5 m below surface. *In situ* parameters (pH, dissolved oxygen, conductivity, redox

348   potential and temperature) were measured using a *YSI 556 MPS* probe, a few centimeters

349   downstream of the sampling point. A 7.32 m *NASCO Swing Sampler* telescopic pole

350   equipped with a 1 L HDPE bottle was used to collect samples from the banks of small

351   rivers and streams. The perch and its container were rinsed on site at a point located a few

352   meters downstream of the sampling site. Whenever sampling from a bridge was possible,

353   the samples were collected using 1 L *Waterra ecobailer*s. A nylon wire equipped with a

354   float was attached to the bailer to indicate the sampling depth. The bailers were

355   systematically rinsed on site, with water from rivers prior to sampling. Some of the

356   streams and rivers were sampled immediately at the outlet of large lakes (Table 3). These

357   samples are used to provide an instantaneous estimate of the isotopic composition of

358   water in the epilimnon at the outlet of the lake. Grab samples were also collected from 16

359   additional lakes, including 14 kettle lakes (Table 3). The samples from Lake

360   Témiscamingue were collected from a boat, at a depth of 1 m using a *NASCO Swing*

361   *Sampler* telescopic pole equipped with a 1 L HDPE bottle. The samples from Lake Tee

362   were collected from a boat, approximately 1 m below the surface, using a plastic tubing

363   equipped with an inertial valve. The samples from kettle lakes were collected from the

364   shoreline, approximately 1 m below surface, using a *NASCO Swing Sampler* telescopic

365   pole equipped with a 1 L HDPE bottle.

366   **Table 3. Summary of surface waters sampling conditions**

367   All surface water samples were filtered immediately after collection using 0.45 µm

368   *Waterra FHT*. The samples collected for stable isotopes analyses (δ^2H-δ^{18}O) were stored

369   in 30-60 ml HDPE bottles and kept at 4 °C until analysis.

370   *Springs*

371   Groundwater springs were sampled between July 2009 and September 2011 through the

372   course of a previous study (Castelli 2012). These samples are associated with the

373   Vaudray-Joannès, Launay and Saint-Mathieu-Berry eskers and with the Harricana

374   Moraine. Other spring samples were collected during the summer of 2013. These

375   correspond to springs that are equipped for drinking water supply. All spring samples

376   were filtered immediately after collection using 0.45 µm *Waterra FHT* carthridges. The

377   *in situ* parameters (pH, dissolved oxygen, specific electrical conductivity (SEC), redox

378   potential and temperature) were measured on site using a multi-parameter probe. Further

379   details about the sampling methodology can be found in Castelli (2012). The samples

380   collected for stable isotopes analyses (δ^2H-δ^{18}O) were stored in 30-60 ml HDPE bottles.

381   The samples collected for tritium (^{3}H) analyses were stored in 1 L HDPE bottles.

382   Sampling bottles for stable isotopes analyses (δ^2H-δ^{18}O) and tritium (^{3}H) analyses were

383   filled to the top with no head space and kept at 4 °C until analysis.

384   *Groundwater*

385   Municipal, private and observation wells were sampled during this study. The targeted

386   wells were commonly identified using the Quebec Ministry of the Environment water

387   well databases, including the Hydrogeological Information System (HIS).

388   Complementary information about the characteristics of the sampled wells was obtained

389   from the private owners or from municipal employees. Well logs were used to document

390   the characteristics of the sampled observation wells. Two conditions had to be met prior

391   to groundwater samples collection: the infrastructures had to be purged of a minimal

392   volume of water and the monitored *in situ* parameters had to reach predefined stability

393   criteria. Water was therefore systematically purged from domestic and observation wells

394   before sample collection. This procedure allows draining the stagnant water from the

395   infrastructure to obtain a water sample that represents groundwater from the aquifer. For

396   private wells, it was assumed that water was withdrawn on a regular basis and that the

397   minimal purge could be limited to the volume of the pressurized reservoirs. The purging

398   was done from taps supplying untreated water. The minimum purging volume for

399   observation wells corresponded to three times the total volume of water stored within the

400   well and its gravel pack. In municipal wells, it was assumed that water is withdrawn at a

401   sufficient rate to prevent stagnation within infrastructures and that no minimal purge was

402   required. During the purge, *in situ* parameters (pH, dissolved oxygen, SEC, redox

403   potential and temperature,) were measured using a multi-parameter probe. The samples

404   were retrieved only after all of the *in situ* parameters had reached the stability criteria

405   reported in Table 4 for three consecutive measurements separated by five minutes

406   intervals. The samples collected for stable isotopes analyses (δ^2H-δ^{18}O) were stored in

407   30-60 ml HDPE bottles and kept at 4 °C until analysis. The samples collected for tritium

408   (^{3}H) analyses were stored in 1 L HDPE bottles. Sampling bottles for tritium (^{3}H) analyses

409   were filled under water in a bucket and capped under water with no head space following

410   a filling procedure described by the USGS and kept at 4 °C until analysis.

411

412   **Table 4. Stability criteria for groundwater sample collection**
413

414   *Analytical procedures*

415   Water samples were analyzed for δ^2H and $\delta^{18}O$ at the stable isotopes laboratory of the

416   Geotop-UQAM research center in Montreal, Canada. Measurements were made using a

417   dual inlet *Micromass Isoprime*™ isotope ratio mass spectrometer coupled to an

418   *Aquaprep*™ system. For oxygen and hydrogen isotopic analyses, 200 µl of water were

419   transferred into septum vials and equilibrated in a heated rack with a known volume of

420   CO_2 (H_2 in the case of hydrogen analyses, with a platinum catalyst). The isotopic

421   compositions of samples were corrected using internal reference waters ($\delta^{18}O$ = -6.71‰,

422   -13.98‰ and -20.31‰; δ^2H= -51.0‰, -99.0‰ and -155.4‰) calibrated on the VSMOW-

423   SLAP scale (Coplen 1996). Reference waters were systematically analyzed between

424   series of samples in order to check for instrumental stability. The analytical uncertainty is

425   ≤ 1‰ for δ^2H and ≤ 0.05‰ for $\delta^{18}O$ at the 1σ level. Values are reported in permil units

426   (‰) against the Vienna Standard Mean Ocean Water standard (VSMOW). Water samples

427   for tritium (^3H) analyses were measured by liquid scintillation counting (LSC) at the

428   Environmental Isotope Laboratory of the University of Waterloo, Canada. The detection

429   limit for enriched samples is 0.8 tritium units (TU).

430   *Data organization and statistical analyzes*

431   In order to support the interpretation of results, the isotopic data are organized according

432   to the main hydrological components and aquifers that were presented previously

433   (Table 1; Figure 2). Overall, eight distinct groups are identified for segregating the

434   isotopic data. The latter include (with numbers corresponding to those reported in

435   Figure 2) samples corresponding to (1) precipitation, (2) the snowpack, (3) surface

436   waters, (4) springs, (5) unconfined granular aquifers, (6) confined granular aquifers, (7)

437   unconfined fractured rock aquifers and (8) confined fractured rock aquifers. The basic

438   statistical analyses conducted on the dataset and related plots were performed using the

439   *Statistica version 6 (StatSoft Inc., 2004)* and *Microsoft Excel* software.

440

441   **Results and discussion**

442   The entire dataset associated with stable isotopes analyses is shown in Figure 3a, whereas

443   Figure 3b allows a better representation of surface and groundwater data. Figure 3c

444   presents the average values of groundwater and surface water groups in the same range as

445   Figure 3b. As a complement, Figure 4 presents boxplots showing the non-outlier range,

446   25th and 75th percentiles and median SEC, δ^{18}O and ^{3}H values for selected groups of data.

447   The non-outlier range is defined as maximum and minimum values within 1.5 times the

448   interquartile range. It was chosen not to show the data outside of the non-outlier range in

449   the boxplots (Figure 4) in order to allow a better representation of the data. Nevertheless,

450   the entire dataset is shown in Figure 3. Results associated with three of the main

451   components of the water cycle (namely precipitation, surface waters and groundwater)

452   are first discussed separately to address specific topics and jointly interpreted afterward to

453   propose a regional-scale conceptual model of groundwater flow.

454

455   **Figure 3. Isotopic composition of precipitation, surface waters, springs and**

456   **groundwater**

457

458   **Figure 4. δ^{18}O (a; b), ^{3}H (c) and SEC (d) boxplots for precipitation, surface waters,**

459   **springs and groundwater**

460

461   *The isotopic composition of precipitation: air masses and seasonal patterns*

462   The δ^2H and δ^{18}O values of precipitation ranged from -217.9‰ to -29.9‰ and -28.4‰ to

463   -4.8‰ respectively (Figure 3a). These data are used to define the Local Meteoric Water

464   Line, calculated using precipitation (n=164) and snowpack data (n=31) (LMWL; δ^2H =

465   7.84 δ^{18}O + 9.20 ‰ (n = 195, r^2 = 0.99); Figure 3). The LMWL is relatively close to

466   Craig's global meteoric water line (GMWL; δ^2H = 8 δ^{18}O + 10 ‰ SMOW; Craig 1961).

467   In terms of temporal variations, the monthly precipitation data revealed the expected

468   temperature-dependant isotopic cycle, with heavy isotopes depletion during the colder

469 period and enrichment during the warmer period (Figure 5). Such a pattern is typical of

470 boreal regions with summer rains enriched in heavy isotopes and winter precipitation

471 depleted in heavy isotopes in response to strong seasonal variations in temperature (Clark

472 and Fritz 1997). Overall, the temporal variations in the isotopic composition of

473 precipitation reflect the marked seasonality of the study area.

474 The weighted mean annual isotopic compositions of precipitation at stations 1, 3 and 4

475 are shown in Table 5. The data do not show a clear relationship between precipitation

476 δ^2H-δ^{18}O and latitude. The absence of a latitudinal gradient in precipitation isotopic

477 composition could reflect the superimposed influence of the three major air masses that

478 supply moisture over the study area, namely (1) the Arctic air mass (from the north),

479 (2) the tropical vapor (from the south) and (3) the westerlies (Bryson 1966; Fritz et al.

480 1987). Given the relatively flat landscape of the study area, the effect of altitude on

481 precipitation δ^2H-δ^{18}O values is probably limited. Finally, evaporation processes might

482 also influence the isotopic composition of precipitation at the local scale, near large water

483 bodies such as the Témiscamingue, Simard and Abitibi lakes (Figure 1). Further data

484 would be required to better explain spatial variations in the isotopic composition of

485 precipitations at the scale of the study area.

486 Samples collected from the snowpack in March 2014 (prior to the onset of spring

487 snowmelt) revealed δ^2H and δ^{18}O values ranging from -184.4‰ to -151.6‰ and –24.5‰

488 to –20.6‰ respectively (Figure 3). Ice layers have been found in some places in the

489 snowpack during sample collection. It is recognized that isotopic fractionation occurs

490 during snowmelt (Taylor et al. 2001; Laudon et al. 2002). This suggests that the different

491 layers identified within the sampled snowpack (which reflect melting / refreezing events)

492 are most likely characterized by variable isotopic compositions. Nevertheless, here, the

493 bulk samples (i.e. composite samples of the entire thickness of snow) collected from the

494 snowpack prior to the onset of the snowmelt event plot uniformly on the left side of the

495 LMWL (Figure 3), with values similar to that measured at the precipitation monitoring

496 stations. This suggests that the bulk of the snowpack preserved an isotopic composition

497 that is similar to that of precipitation prior to the onset of the spring snowmelt event.

498   Overall, the isotopic compositions of samples retrieved from the snowpack do not define

499   a clear latitudinal gradient at the regional scale.

500

501   **Table 5. Amount weighted average isotopic composition of precipitation at the four**
502   **sampling stations (2013-2015).**
503

504   **Figure 5. Seasonal variations in precipitation amounts and δ^{18}O composition**

505

506   *The isotopic composition of surface waters: inflows, evaporative enrichment and mixing*

507   The regional dataset reveals a significant variability in surface waters δ^2H and δ^{18}O, with

508   values ranging from -100.8‰ to -68.9‰ and -13.7‰ to -7.6‰, respectively (for regional

509   average values of -80.9‰ (δ^2H) and -10.7‰ (δ^{18}O)). The isotopic composition of surface

510   waters can present both spatial and temporal variations owing to the superimposed

511   influence of precipitation, groundwater inflow, evaporation and tributary mixing

512   processes (Yi et al. 2010). Temporal variations are commonly observed in regions

513   characterized by a marked seasonality where heavy isotope depletion following snowmelt

514   and enrichment caused by evaporation during the ice off period have been reported (e.g.

515   see Telmer and Veizer 2000; Yi et al. 2010). Here, most of the samples were collected in

516   summer (Table 2), and the data plot below the LMWL, consistent with the hypothesis

517   that surface waters have undergone heavy isotope enrichment owing to evaporation. A

518   surface Local Evaporation Line (LEL): δ^2H = 3.80 δ^{18}O – 40.22 ‰ (n = 99, r^2 = 0.65)

519   (Figure 3a) is evaluated from the data. The evaporation over inflow ratio (E/I), as

520   described by Gibson and Edwards (2002), corresponds to the water balance of a surface

521   water body and relates to the combined effects of evaporative heavy isotope enrichment

522   and dilution by inflowing waters. The E/I ratio is used here for evaluating the

523   hydrological processes responsible for the distribution of surface water data plotting

524   below the LMWL in δ^2H vs δ^{18}O graphs (Figure 3). The *Hydrocalculator* application

525   from Skrzypek et al. (2015) was used to calculate evaporation over inflow (E/I) ratios

526   under steady state conditions (shown over the LEL in Figure 6a). This application solves

527   a modified form of the Craig and Gordon (1965) model:

528    $$\frac{E}{I} = \left[\frac{(\delta_L - \delta_P)}{(\delta^* - \delta_L) \times m} \right]$$ Equation 2

529   Where δ_L corresponds to the isotopic composition of the sampled surface water, δ_P is the

530   initial isotopic composition of water and δ^* is the limiting isotopic enrichment factor (a

531   function of the isotopic fractionation factor and atmospheric isotopic composition and

532   relative humidity). Similar approaches are used to evaluate the E/I ratios of rivers

533   (e.g.: Telmer and Veizer 2000) and lakes (e.g. Gibson and Edwards 2002). Here,

534   theoretical calculations are proposed for points falling directly on the LEL evaluated from

535   the dataset, the latter corresponding to the δ_L term of equation 2. The initial isotopic

536   composition of water (δ_P) is assumed to correspond to the intersection between the

537   LMWL and the LEL. The isotopic composition of atmospheric moisture (δ_A) , which is

538   needed to evaluate δ^* in equation 2, is evaluated according to three scenarios:

539   1- δ_A is in equilibrium with the flux weighted average isotopic composition of

540   precipitation between the months of May and August (δ_A = -141.21 ‰ ; -19.45

541   ‰);

542   2- δ_A is in equilibrium with the arithmetic average isotopic composition of

543   precipitation between the months of May and August (δ_A= -137.42 ‰ ; -18.91

544   ‰);

545   3- δ_A is in equilibrium with δ_P (δ_A= -156.03 ‰ ; -21.63 ‰).

546   A temperature of 22 °C and a relative humidity of 70% are assumed, consistent with the

547   conditions encountered during the warm ice off period within the study region. The

548   isotope fractionation factors are calculated from the Horita and Wesolowski (1994)

549   equations.

550   Depending on the model parameters used, E/I ratios ranging between 0% and 36% are

551   evaluated from the regional dataset (Figure 6a). Based on this theoretical framework,

552   surface water samples plotting closer to the LMWL most likely present the lowest E/I

553 ratios. These surface waters might be affected by significant evaporation losses, but
554 inflows (mostly precipitation and groundwater, both plotting along the LMWL) are
555 sufficient to buffer the heavy isotope enrichment resulting from evaporation. On the
556 contrary, the samples that are most enriched in heavy isotopes (i.e. plotting further along
557 the right side of the LEL) most likely present the highest E/I ratios. Within the regional
558 hydrogeological framework, it is most likely that evaporation mainly occurs within lakes
559 and stagnant water bodies whereas dynamic in stream processes mainly reflect surface
560 water / groundwater interactions and tributary mixing.

561 One distinctive feature of the regional dataset is that most of the kettle lakes plot on the
562 right side of the LEL, suggesting overall high E/I ratios in comparison to other surface
563 waters (Figure 6b). Recent studies by Isokangas et al. (2015) and Arnoux et al. (2017)
564 provided novel methods to estimate the groundwater dependency of such lakes based on
565 E/I ratios calculated from stable isotope data, among other. Here, quantifying the
566 groundwater dependency of lakes is precluded by uncertainties related to volumes,
567 surface water inflows and potential heterogeneities caused by thermal stratification and
568 temporal variations. Nevertheless, the distinctive isotopic composition of kettle lakes
569 stresses the need for conducting further studies aimed at quantifying their water balance
570 to better anticipate their sensitivity to climate change and human pressure.

571

572 **Figure 6. Interpretation of the isotopic compositions of surface waters**

573

574 *The isotopic composition of groundwater and springs: recharge, discharge, mixing and regional*
575 *flowpaths*

576 The stable isotopes analyses (δ^2H-δ^{18}O) conducted on 351 groundwater and springs
577 samples are shown on the graphs of Figures 3, 4a and 4b. The data associated with
578 groundwater samples are represented according to the four main types of regional
579 aquifers, as shown in Figure 2 (unconfined granular aquifers; unconfined fractured rock
580 aquifers; confined granular aquifers; confined fractured rock aquifers). The δ^2H and δ^{18}O
581 values of groundwater samples ranged from -107.8‰ to -71.9‰ and -15.2‰ to -9.4‰,

582   respectively, for a regional average of -13.3‰ (δ^{18}O); -93.4‰ (δ^{2}H). The δ^{2}H and δ^{18}O

583   values of spring samples ranged from -106.3‰ to -75.1 ‰ and -14.4‰ to -9.7‰,

584   respectively for a regional average of -13.8‰ (δ^{18}O); -98.1‰ (δ^{2}H). Previous work by

585   Castelli (2012) revealed that the isotopic composition of springs is fairly stable

586   (1) throughout the ice-off season and (2) from year to year. Similarly, it is assumed here

587   that the isotopic composition of groundwater is relatively constant in time. The focus is

588   therefore set on spatial rather than temporal variations in isotopic compositions. The data

589   associated with groundwater and springs are evenly distributed around the LMWL. This

590   suggests that (1) infiltration and recharge processes are not significantly affected by

591   evaporation losses and (2) aquifers are not significantly affected by inflows from

592   evaporated surface waters. This is consistent with the regional hydrogeological

593   framework because: (1) the main recharge areas consist of coarse grained glaciofluvial

594   formations where high infiltration rates prevent surface pounding (and associated

595   evaporation) and (2) physical measurements suggest that groundwater generally

596   discharges into surface waters at the regional scale (Cloutier et al. 2013; 2015). Although

597   water losses by plant transpiration prior to groundwater recharge might be significant, the

598   available dataset does not allow the quantification of this process. Results also support

599   the hypothesis that regional surface waters – groundwater interactions are essentially

600   restricted to groundwater discharging into surface waters, and not the inverse (otherwise,

601   some groundwater samples would most likely be plotting significantly below the LMWL

602   owing to mixing with evaporated surface waters). The data do not show systematic

603   latitudinal trends in the stable isotope composition of groundwater at the regional scale.

604   This is most likely caused by the complex mixing of recharge originating from the main

605   atmospheric air masses supplying precipitation over the study region.

606   The data associated with the four main types of aquifers present a significant dispersion

607   and overlap within Figures 3 and 4b. Nevertheless, two main observations arise from the

608   distribution of data within the δ^{2}H-δ^{18}O plots:

609   (1) The data associated with unconfined granular aquifers present a greater

610   dispersion in comparison to the other types of aquifers (Figure 4b);

611   (2) Confined granular aquifers and fractured rock aquifers (both confined and
612   unconfined) tend to plot further on the right side of LMWL in comparison to
613   springs and unconfined granular aquifers (Figure 3c).

614   These observations are interpreted in an effort to further constrain the understanding of
615   regional flowpaths within the hydrogeological environment conceptually represented in
616   Figure 2. The unconfined granular aquifers represent the main regional recharge zones
617   where rain and melted snow preferentially infiltrate at different periods of the year,
618   depending on local climatic and hydrological conditions (Cloutier et al. 2016). The
619   proposed interpretation of groundwater stable isotope data is that unconfined granular
620   aquifers present a greater δ^2H-δ^{18}O variability owing to a shorter residence time of water
621   within shallow and dynamic systems such as eskers and moraines. The results associated
622   with ^{3}H analyzes (Figure 4c) further support this interpretation. Overall, the tritium data
623   suggest that water samples from springs, unconfined granular aquifers and unconfined
624   fractured rock aquifers correspond to modern waters (with values ranging between
625   approximately 9 and 17 TU, consistent with the subdivisions proposed by Clark and Fritz
626   1997). Such results suggest a relatively short residence time of water in these shallow
627   components. In contrast, samples collected within confined aquifers (both granular and
628   fractured) present tritium contents below 0.8 TU (consistent with submodern values
629   according to the subdivisions proposed by Clark and Fritz 1997). Such results suggest
630   that within the region, confined aquifers generally contain older groundwater in
631   comparison to unconfined aquifers.

632   The sampled springs are all located on the flanks of unconfined granular aquifers
633   associated with glaciofluvial formations (eskers / moraines). Their heavy isotope
634   depletion (Figure 3c) with respect to most groundwater samples suggests that superficial
635   flow systems associated with springs are submitted to a greater influence of lighter
636   precipitation. As previously discussed, within the study area, precipitations depict a clear
637   seasonal pattern, with lighter values recorded during the cold period (Figure 5). Under
638   such conditions, one likely explanation is that a significant proportion of the groundwater
639   recharge associated with snowmelt contributes to springs discharge. This stands as a
640   plausible explanation because the springs located on the flanks of eskers and moraines

641   essentially consist in «overflows» allowing groundwater to discharge from unconfined

642   granular aquifers towards the surface water network. From a physical perspective, it

643   seems likely that «overflow» conditions would be favored following the thawing period,

644   as groundwater levels are generally raising within the eskers and moraines of the region

645   during this period (Cloutier et al. 2013; 2015). During the dryer summer period, recharge

646   rates are likely reduced, therefore limiting the supply of heavier water associated with

647   summer precipitation to shallow flow systems. In fall, at the end of the warmer period,

648   when the uptake of water by vegetation is reduced and precipitation are increased,

649   recharge rates most likely increase, further supplying water that is depleted in heavy

650   isotopes to the shallow flow systems associated with springs. The loss of lighter isotopes

651   resulting from groundwater discharge within springs could also partly explain why the

652   confined aquifers, located further downstream within the flow systems, are slightly

653   enriched in heavy isotopes with respect to springs and shallow unconfined aquifers

654   (Figures 3c; 4b). One key regional observation discussed by Cloutier et al. (2016) is that

655   extensive peatlands are developed on the flanks of several eskers and moraines of the

656   region. The contacts between esker/moraines and these extensive peatlands are

657   interpreted as diffuse groundwater seepage zones (Nadeau et al. 2015). The process

658   related to the loss of lighter isotopes within punctual springs might therefore be

659   generalized to most of the unconfined aquifers associated with extensive peatlands and

660   diffuse groundwater seepage zones. In addition, it seems most likely that the areas

661   associated with unconfined fractured rock aquifers are less prone to groundwater

662   recharge during snowmelt in comparison to the areas associated with glaciofluvial

663   formations (i.e. unconfined granular aquifers). This hypothesis is based on the contrast in

664   hydraulic conductivity (K) between the fractured bedrock (lower K) and the eskers and

665   moraines (higher K) (e.g. see Cloutier et al. 2015). The differences in the isotopic

666   composition of unconfined granular aquifers and springs compared to that of confined

667   granular aquifers and fractured rock aquifers (both confined and unconfined) could

668   therefore reflect the relative contribution of snowmelt induced recharge for the different

669   types of aquifers.

670   The interpretations discussed above are further illustrated in Figure 7a, where the SEC of

671   springs and groundwater is plotted against the corresponding $\delta^{18}O$ values. The data

672   presented therein reveals that confined fractured rock aquifers generally present the

673   highest SEC values whereas the unconfined granular aquifers present the lowest SEC

674   values. This is also depicted in Figure 4d where a gradual increase in SEC is observed

675   from unconfined towards confined aquifers. SEC can thus be used as a proxy for

676   groundwater residence time and geochemical evolution, higher SEC generally implying

677   more evolved groundwater. This pattern most likely reflects the combined effects of

678   (1) increased geochemical interactions between groundwater and the geological

679   environment along regional flowpaths and (2) recharge of precipitation having very low

680   dissolved solid concentration (thus quite low SEC) in unconfined granular aquifers areas.

681   The mixing model shown in Figure 7a further supports the interpretations proposed

682   above. Three end-members are proposed to explain the variability in both $\delta^{18}O$ and SEC

683   values:

684   1- End-member «A» presents low SEC and $\delta^{18}O$, it is identified as representative of

685   recent snowmelt induced recharge. The lowest non-outlier $\delta^{18}O$ value recorded in

686   unconfined granular aquifers (lower end of the boxplot shown in Figure 4b) is

687   used to characterize this end-member, whereas the SEC value is set to 0.05

688   mS/cm, corresponding to the lowest non-outlier SEC value recorded in

689   unconfined granular aquifers (lower end of the boxplot shown in Figure 4d);

690   2- End-member «B» presents low SEC and high $\delta^{18}O$ close to -12‰, it is identified

691   as representative of fall recharge affected by relatively high temperature rain. The

692   highest non-outlier $\delta^{18}O$ value recorded in unconfined granular aquifers (higher

693   end of the boxplot shown in Figure 4b) is used to characterize this end-member,

694   whereas the SEC value is set to 0.05 mS/cm, as previously defined for end-

695   member «A»;

696   3- End-member «C» presents high SEC and $\delta^{18}O$, it is identified as representative of

697   well mixed water (from various recharge zones or various recharge periods) that

698   is geochemically evolved owing to prolonged water-rock interactions along

699   flowpaths, thus leading to a higher SEC. The median $\delta^{18}O$ isotopic composition of

700   confined fractured rock aquifers is used to constrain this end-member, and the

701   SEC is set to 1.8 mS/cm (the highest recorded value in the dataset, Figure 4d).

702   The dashed lines in figure 7 a and b represent mixing lines between the three end-
703   members, at 25% intervals. In this mixing model, the SEC is considered linearly related
704   to the geochemical level of evolution of groundwater, which is most probably not linearly
705   related to the groundwater residence time.

706   Six main outliers are identified among the groundwater/springs dataset in Figures 3b.
707   These six points plot below the LMWL in Figure 3, suggesting an evaporative
708   enrichment that is not observed in the other groundwater samples. Five of these points are
709   associated with samples collected in the immediate vicinity of lakes whereas the fifth one
710   was collected within a mining site. It is proposed that the five samples collected near
711   lakes and presenting heavy isotope enrichment and low SEC values are directly affected
712   by the supply of evaporated and low SEC lake waters. The wells characterized by low
713   SEC and low δ^{18}O values are likely affected by nearby snowmelt induced groundwater
714   recharge, whereas those with low SEC and significantly higher δ^{18}O values are likely
715   affected by mixing with surface waters. In that sense, within the study region, stable
716   isotope data could be used as a screening tool to detect groundwater wells that are
717   affected by surface waters. Such wells would deserve a specific attention in groundwater
718   monitoring programs because they might be more vulnerable to microbial contamination
719   originating from surface waters. Finally, the sixth outlier point was collected in a
720   groundwater well located within a mining site; its isotopic composition and SEC value
721   most likely reflect anthropogenic effects.

722

723   **Figure 7. Specific electrical conductivity (SEC) vs δ^{18}O of springs, surface waters**
724   **and groundwater**

725

726   *Local and regional systems of groundwater flow: insights from water stable isotopes*

727   Tóth (1963) proposed a conceptual model of groundwater flow in 2D cross sections
728   involving local, intermediate and regional groundwater flow sub-systems. Such
729   conceptual models constitute a central unifying concept to describe groundwater

730 recharge, flow and discharge processes at various scales and provide a framework that is

731 of upmost importance to interpret regional hydrogeochemical datasets. Tóth (1999)

732 further developed his conceptual model by presenting groundwater as a geologic agent

733 interacting with the environment and inheriting a geochemical composition that preserves

734 an archive of hydrogeochemical processes and systematically evolves along flow paths.

735 Following Toth's pioneer work, the different flow systems of the study area are

736 interpreted with a focus on the isotopes of the water molecule itself, rather than other

737 dissolved species. The working hypothesis is that within the considered spatiotemporal

738 domain, the isotopic composition (δ^2H-δ^{18}O) of water is not significantly affected by

739 water-rock interactions but rather mainly reflects the superimposed effects of

740 precipitation isotopic composition, evaporation, recharge, mixing and discharge

741 processes that vary in time and space. The average δ^2H-δ^{18}O compositions of

742 precipitation (including snow samples), surface waters, springs and groundwater are

743 shown in Figure 8, which consists in a more detailed representation of the regional

744 hydrogeological conditions that was initially conceptualized in Figure 2.

745 The conceptual model illustrates precipitation showing the greatest isotopic variability

746 and recharge occurring mainly within shallow unconfined aquifers, where the variability

747 in the isotopic composition of water is attenuated with respect to precipitation due to

748 mixing. Part of the water flowing within these unconfined aquifers discharges towards

749 surface waters through springs and diffuse seepage zones that are generally depleted in

750 heavy isotopes with respect to the average composition of groundwater. Surface waters

751 are subsequently submitted to evaporation (causing heavy isotope enrichments) and to

752 further dilution by precipitation and groundwater discharge. The remaining groundwater

753 flows from unconfined recharge areas towards confined aquifers, allowing two key

754 geochemical processes to occur along flow paths:

755 (1) Water rock interaction: groundwater becomes increasingly concentrated in

756   dissolved ions owing to prolonged water-rock interactions, as shown by the

757   gradual increase in SEC among the various hydrological components, from

758   precipitations towards confined fractured rock aquifers (Figure 4d). This

759   interpretation is further supported by the tritium analyses (Figure 4c), which

760   suggest that confined aquifers are characterized by longer water residence times
761   compared to springs and unconfined aquifers;

762   (2) Mixing: The isotopic composition of groundwater evolves towards a regional
763   average owing to the mixing of water originating from various recharge zones or
764   various recharge periods. This is illustrated in Figure 4b and Figure 7a, which
765   suggest that mixing processes tend to damp the variability recorded in $\delta^{18}O$ values
766   within confined aquifers. In other terms, the greater the proportion of unconfined
767   aquifers in the vicinity on a given site, the greater the potential variability in the
768   stable isotope composition of groundwater.

769   Clark and Fritz (1997) proposed a schematic representation of the attenuation of seasonal
770   isotope variations in recharge waters within the unsaturated zone. These authors reported
771   that temporal isotopic variations around an average value are gradually damped with
772   increasing depth as a function of flowpaths lengths and residence times. A comparable
773   interpretation is proposed here to explain the evolution of groundwater SEC and
774   δ^2H-$\delta^{18}O$ along local, intermediate and regional flow systems (Figures 7 and 8). On one
775   hand, since recharge processes are primarily associated with sectors of unconfined
776   aquifers and partly controlled by hydrogeological conditions that are highly
777   heterogeneous at the regional scale, a significant variability is recorded in unconfined
778   aquifers isotopic compositions. Overall, the unconfined granular aquifers associated with
779   coarse grained glaciofluvial formations (eskers and moraines) are more prone to recharge
780   during snowmelt and therefore present low δ^2H-$\delta^{18}O$ values in comparison to the other
781   types of aquifers. Similarly, the springs found on the flanks of eskers and moraines are
782   depleted in heavy isotopes. On the other hand, recharge areas associated with unconfined
783   bedrock aquifers are more prone to runoff generation during the intense snowmelt event,
784   and are therefore generally enriched in heavy isotopes in comparison to unconfined
785   granular aquifers. Finally, the confined aquifers located further along groundwater
786   flowpaths are fed by numerous interconnected unconfined aquifer areas that are
787   heterogeneously distributed over the region. The result of the mixing processes occurring
788   along flowpaths is a gradual evolution towards a regional average value within confined
789   aquifers. Based on this interpretation, groundwater samples from confined aquifers that

790   present an isotopic composition that significantly differs from the regional average most

791   likely represents sites where the preferential influence of a nearby recharge area are

792   recorded.

793

794   **Figure 8. Isotopic variations within local, intermediate and regional flow systems**

795

796   **Conclusions**

797   The isotopic composition of water (δ^2H-δ^{18}O and ^{3}H) in precipitation, surface waters, groundwater

798   and springs was used to improve the understanding of regional flow systems in the southern portion

799   of the Barlow-Ojibway Clay Belt. The data allowed the identification of the key hydrological

800   processes driving spatiotemporal isotopic variations and deciphering the interaction pathways

801   between the various components of the water cycle, from atmospheric moisture to groundwater

802   discharge:

803   (1) Regional precipitations depict a clear seasonal pattern with heavy isotope depletion

804   recorded in winter and heavy isotope enrichment in summer. The data did not reveal clear

805   spatial trends in precipitation δ^2H-δ^{18}O, most likely in response to the complex mixing of

806   inputs from the main air masses supplying moisture to the study region. Overall,

807   precipitation data allowed the definition of the local meteoric water line (LMWL:

808   δ^2H = 7.84 δ^{18}O + 9.20 ‰ ; n = 164; r^2 = 0.99);

809   (2) Surface waters plot below the LMWL in a δ^2H-δ^{18}O graph owing to evaporation losses.

810   Calculations conducted using a modified form of the Craig and Gordon (1965) model with

811   the *Hydrocalculator* application (Skrzypek et al. 2015) provided an estimation of

812   evaporation over inflow (E/I) ratios ranging between 0% and 36% at the regional scale;

813   (3) Groundwater samples plot on the LMWL and are evenly distributed around the average

814   isotopic composition of precipitation in a δ^2H-δ^{18}O graph, suggesting that evaporation

815   processes do not significantly affect regional recharge waters. The δ^2H-δ^{18}O of

816   groundwater in shallow unconfined aquifers presents a greater variability in comparison to

817   confined aquifers owing to mixing processes that tend to buffer the isotopic variability

818   along the regional groundwater flow paths. This buffering on the isotopic composition

819   variability is accompanied by increasing values of the SEC of groundwater from

820   unconfined to confined aquifers, most likely in response to increasing water-rock

821   interaction timescales, consistent with generally lower tritium contents in confined aquifers;

822   (4) Unconfined granular aquifers and associated springs are generally slightly depleted in

823   heavy isotopes in comparison to other groundwater samples, suggesting that these shallow

824   flow systems are preferentially recharged during spring snowmelt within the region.

825   Overall, the observations and interpretations of this study support an improvement of a conceptual

826   hydrogeological model of local and regional hydrological systems and flow paths that is consistent

827   with the geological framework. This conceptual model illustrates how water isotopes can be used to

828   constrain physically-based interpretations of local, intermediate and regional flow systems such as

829   those inspired by the pioneering work of Tóth (1963), even in a highly heterogeneous region.

830   The buffering of isotopic variability in groundwater from groundwater recharge areas

831   located in unconfined aquifers towards groundwater discharge areas and confined

832   aquifers located further along regional flow paths provides a framework for deciphering

833   the processes associated with the geochemical evolution of groundwater, as a

834   complement to understandings based on dissolved major ions and trace elements.

835

850

851 **References**

852 Araguás-Araguás, L., K. Froehlich, and K. Rozanski. 2000. Deuterium and oxygen-18
853   isotope composition of precipitation and atmospheric moisture. *Hydrological*
854   *Processes* 14(8): 1341-1355.

855 Arnoux, M., F. Barbecot, E. Gibert-Brunet, J. Gibson, E. Rosa, A. Noret, and G.
856   Monvoisin. 2017. Geochemical and isotopic mass balances of kettle lakes in
857   southern Quebec (Canada) as tools to document variations in groundwater quantity
858   and quality. *Environmental Earth Sciences* 76(3): 106.

859 Asselin, M. 1995. L'Abitibi-Témiscamingue: trois sous-régions, une région. Chap. 1 in
860   *Histoire de l'Abitibi-Témiscamingue* (sous la direction de Odette Vincent), ed.
861   Institut québécois de recherche sur la culture, 21-65. Québec, Canada.

862 Birks, S.J., and J.J. Gibson. 2009. Isotope Hydrology Research in Canada, 2003-2007.
863   *Canadian Water Resources Journal* 34(2): 163-176.

864 Bryson, R.A. 1966. Air masses, streamlines and the boreal forest. *Geographical Bulletin*
865   8(3): 228-269.

866 Bryson, R.A., and F.K. Hare. 1974. The Climates of North America. Chap. 1 in *Climates*
867   *of North America*, in *World Survey of Climatology* 2 vols, ed. R.A. Bryson, and
868   F.K. Hare, 1-47. Amsterdam-London-New York: Elsevier Publishers.

869 Castelli, S. 2012. Hydrogéochimie des sources associées aux eskers de l'Abitibi, Québec.
870   Maîtrise, Département des génies civil, géologique et des mines, école
871   polytechnique de Montréal, Université de Montréal, 126 pp.

872 Clark, I. D. and Fritz, P., 1997. *Environmental Isotopes in Hydrogeology*. CRC Press,
873   Boca Raton (London), New York, 328 pp.

874 Cloutier, V., D. Blanchette, P.-L. Dallaire, S. Nadeau, E. Rosa, and M. Roy. 2013. *Projet*
875   *d'acquisition de connaissances sur les eaux souterraines de l'Abitibi-Témiscamingue*
876   *(partie 1)*. Rapport final. Groupe de recherche sur l'eau souterraine. Institut de

877   recherche en mines et en environnement. Université du Québec en Abitibi-
878   Témiscamingue, 151 pp.

879   Cloutier, V., D. Blanchette, P.-L. Dallaire, S. Nadeau, E. Rosa, and M. Roy. 2015. *Projet*
880   *d'acquisition de connaissances sur les eaux souterraines de l'Abitibi-*
881   *Témiscamingue (partie 2)*. Rapport final. Groupe de recherche sur l'eau souterraine,
882   Institut de recherche en mines et en environnement, Université du Québec en
883   Abitibi-Témiscamingue, 313 pp.

884   Cloutier, V., E. Rosa, M. Roy, S. Nadeau, D. Blanchette, P.-L. Dallaire, G. Derrien, and
885   J.J. Veillette. 2016. *Atlas hydrogéologique de l'Abitibi-Témiscamingue*. Québec :
886   Presses de l'Université du Québec, 77 pp.

887   Collini, M., L. Germain, and J. Thibeault. 2007. *Portrait des ressources hydriques*.
888   Observatoire de l'Abitibi-Témiscamingue. Les portraits de la région, 47 pp.

889   Coplen, T.B. 1996. New guidelines for reporting stable hydrogen, carbon, and oxygen
890   isotope-ratio data. *Geochimica et Cosmochimica Acta* 60(17): 3359-3360.

891   Craig, H. 1961. Isotopic variations in meteoric waters. *Science* 133(3465): 1702-1703.

892   Craig, H., and L.I. Gordon. 1965. Deuterium and oxygen 18 variations in the ocean and
893   marine atmosphere. In *Stable Isotopes in Oceanographic Studies and*
894   *Paleotemperatures*, 1965, Spoleto, Italy, ed. E. Tongiorgi, 9-130. Laboratorio di
895   Geologia Nucleare: Pisa.

896   Dansgaard, W. 1964. Stable isotopes in precipitation. *Tellus* 16(4): 436-468.

897   Ferguson, P.R., N. Weinrauch, L.I. Wassenaar, B. Mayer, and J. Veizer. 2007. Isotope
898   constraints on water, carbon, and heat fluxes from the northern Great Plains region
899   of North America. *Global biogeochemical cycles* 21(2).

900   Fritz, P., R. Drimmie, S. Frape, and K. O'shea. 1987. The isotopic composition of
901   precipitation and groundwater in Canada. In *Isotope techniques in water resources*

902   *development.* Proceedings of a symposium, 30 March - 3 April 1987. International
903   Atomic Energy Agency: Vienna, Austria.

904   Gat, J.R. 1996. Oxygen and hydrogen isotopes in the hydrologic cycle. *Annual Review of*
905   *Earth and Planetary Sciences* 24(1): 225-262.

906   Gat, J.R., C.J. Bowser, and C. Kendall. 1994. The contribution of evaporation from the
907   Great Lakes to the continental atmosphere: estimate based on stable isotope data.
908   *Geophysical Research Letters* 21(7): 557-560.

909   Gibson, J.J., and T.W.D. Edwards. 2002. Regional water balance trends and evaporation-
910   transpiration partitioning from a stable isotope survey of lakes in northern Canada.
911   *Global Biogeochemical Cycles* 16(2): 10-1-10-14.

912   Gibson, J.J., T.W.D. Edwards, S.J. Birks, N.A. St Amour, W.M. Buhay, P. McEachern,
913   B.B. Wolfe, and D.L. Peters. 2005. Progress in isotope tracer hydrology in Canada.
914   *Hydrological Processes* 19(1): 303-327.

915   Green, T.R., M. Taniguchi, H. Kooi, J.J. Gurdak, D.M. Allen, K.M. Hiscock, H. Treidel,
916   and A. Aureli. 2011. Beneath the surface of global change: Impacts of climate
917   change on groundwater. *Journal of Hydrology* 405(3–4): 532-560.

918   Hare, F.K., and J.E. Hay. 1974. The Climate of Canada and Alaska. Chap. 2 in *Climates*
919   *of North America*, in *World Survey of Climatology* 11 vols, ed. R.A. Bryson, and
920   F.K. Hare, 49-192. Amsterdam-London-New York: Elsevier Publishers.

921   Horita, J., and D.J. Wesolowski. 1994. Liquid-vapor fractionation of oxygen and
922   hydrogen isotopes of water from the freezing to the critical temperature.
923   *Geochimica et Cosmochimica Acta* 58(16): 3425-3437.

924   Isokangas, E., K. Rozanski, P.M. Rossi, A.K. Ronkanen, and B. Kløve. 2015.
925   Quantifying groundwater dependence of a sub-polar lake cluster in Finland using
926   an isotope mass balance approach. *Hydrology and Earth System Sciences* 19(3):
927   1247-1262.

928   Jeelani, G., U. Saravana Kumar, and B. Kumar. 2013. Variation of δ18O and δD in
929   precipitation and stream waters across the Kashmir Himalaya (India) to distinguish
930   and estimate the seasonal sources of stream flow. *Journal of Hydrology* 481: 157-
931   165.

932   Kebede, S., Y. Travi, and K. Rozanski. 2009. The δ18O and δ2H enrichment of Ethiopian
933   lakes. *Journal of Hydrology* 365(3–4): 173-182.

934   Kortelainen, N.M., and J.A. Karhu. 2004. Regional and seasonal trends in the oxygen and
935   hydrogen isotope ratios of Finnish groundwaters: a key for mean annual
936   precipitation. *Journal of Hydrology* 285(1–4): 143-157.

937   Laudon, H., H.F. Hemond, R. Krouse, and K.H. Bishop. 2002. Oxygen 18 fractionation
938   during snowmelt: Implications for spring flood hydrograph separation. Water
939   Resources Research 38(11): 40-1-40-10.

940   MAMROT (Ministère des Affaires municipales et de l'Occupation du territoire,
941   Gouvernement du Québec). 2016. *Répertoire des municipalités, Abitibi-*
942   *Témiscamingue,   Québec.*   http://www.mamrot.gouv.qc.ca/repertoire-des-
943   municipalites/fiche/region/08/ (accessed May 2016).

944   MRNF (Ministère des Ressources naturelles et de la Faune). 2006. *Portrait Territorial*
945   *Abitibi-Témiscamingue*, 88 pp.

946   Nadeau, S., E. Rosa, and V. Cloutier. 2017. Accepted: Article ID : TCWR 1354722.
947   Stratigraphic sequences map for groundwater assessment and protection of
948   unconsolidated aquifers: A case example in the Abitibi-Témiscamingue region,
949   Québec, Canada. *Canadian Water Resources Journal.*

950   Nadeau, S., E. Rosa, V. Cloutier, R.-A. Daigneault, and J. Veillette. 2015. A GIS-based
951   approach for supporting groundwater protection in eskers: Application to sand and
952   gravel extraction activities in Abitibi-Témiscamingue, Quebec, Canada. Part B.
953   *Journal of Hydrology*: *Regional Studies* 4: 535-549.

954 Paradis, S.J. 2005. Géologie des formations en surface et histoire glaciaire, Lac
955   Castagnier, Québec. Geological Survey of Canada, Map 1991A, scale 1:100,000.

956 Paradis, S.J. 2007. Géologie des formations en surface et histoire glaciaire, Lac Blouin,
957   Québec. Geological Survey of Canada, Map 2017A, scale 1:100,000.

958 Poirier, C., T. Fortier-Filion, R. Turcotte, and P. Lacombe. 2012. *Apports verticaux*
959   *journaliers estimés de 1900 à 2010, version 2012*. Contribution au Programme
960   d'acquisition de connaissances sur les eaux souterraines. Centre d'expertise
961   hydrique du Québec (CEHQ), Ministère du Développement durable, de
962   l'Environnement et de la Lutte contre les changements climatiques, Ville de
963   Québec, Québec, Canada, 112 pp.

964 Praamsma, T., K. Novakowski, K. Kyser, and K. Hall. 2009. Using stable isotopes and
965   hydraulic head data to investigate groundwater recharge and discharge in a
966   fractured rock aquifer. *Journal of Hydrology* 366(1–4): 35-45.

967 Rouleau, A., J. Guha, G. Archambault, and A. Benlahcen. 1999. Aperçu de
968   l'hydrogéologie en socle précambrien au Québec et des problématiques minières.
969   *Hydrogéologie* 4: 23-31.

970 Rozanski, K., L. Araguàs-Araguàs, and R. Gonfiantini. 1993. Isotopic patterns in modern
971   global precipitation. *Climate Change in Continental Isotopic Records* 78: 1-36.

972 Siegel, D., and R. Mandle. 1984. Isotopic evidence for glacial meltwater recharge to the
973   Cambrian-Ordovician aquifer, north-central United States. *Quaternary Research*
974   22(3): 328-335.

975 Skrzypek, G., A. Mydłowski, S. Dogramaci, P. Hedley, JJ. Gibson, and PF. Grierson.
976   2015. Estimation of evaporative loss based on the stable isotope composition of
977   water using Hydrocalculator. *Journal of Hydrology* 523, 781–789.

978 StatSoft, Inc. 2004. STATISTICA (Data Analysis software System), Version 6.
979   www.statsoft.com.

980   Taylor, R.G., B. Scanlon, P. Döll, M. Rodell, R. Van Beek, Y. Wada, L. Longuevergne,

981   M. Leblanc, J.S. Famiglietti, and M. Edmunds. 2013. Ground water and climate

982   change. *Nature Climate Change* 3(4): 322-329.

983   Taylor, S., X. Feng, J.W. Kirchner, R. Osterhuber, B. Klaue, and C.E. Renshaw. 2001.

984   Isotopic evolution of a seasonal snowpack and its melt. *Water Resources Research*

985   37(3): 759-769.

986   Telmer, K. and J. Veizer. 2000. Isotopic constraints on the transpiration, evaporation,

987   energy, and gross primary production Budgets of a large boreal watershed: Ottawa

988   River Basin, Canada. *Global Biogeochemical Cycles* 14(1): 149-165.

989   Thibaudeau, P., and J.J. Veillette. 2005. Géologie des formations en surface et histoire

990   glaciaire, Lac Chicobi, Québec. Geological Survey of Canada, Map 1996A, scale

991   1:100,000.

992   Thornthwait, C.W. 1944. Report of committee on transpiration and evaporation. Am.

993   Gephys. Union Trans. Part 5 : 686-693.

994   Tóth, J. 1963. A theoretical analysis of groundwater flow in small drainage basins.

995   *Journal of geophysical research* 68(16): 4795-4812.

996   Tóth, J. 1999. Groundwater as a geologic agent: An overview of the causes, processes,

997   and manifestations. *Hydrogeology Journal* 7(1): 1-14.

998   Veillette, J., A. Maqsoud, H. De Corta, and D. Bois. 2004. Hydrogéologie des eskers de

999   la MRC d'Abitibi, Québec. In *Proceedings 57th Canadian Geotechnical*

1000   *Conference, 5th Joint CGS/IAH-CNC Conference*. Québec city, Canada, October

1001   24-27, 2004, pp. 6-13.

1002   Veillette, J.J. 1986. Surficial geology, New Liskeard, Ontario-Quebec. Geological Survey

1003   of Canada, Map 1639A, scale 1:100,000.

1004   Veillette, J.J. 1987a. Surficial geology, Grand Lake Victoria North, Quebec. Geological

1005   Survey of Canada, Map 1641A, scale 1:100,000.

1006   Veillette, J.J. 1987b. Surficial geology, Lac Simard, Quebec. Geological Survey of
1007   Canada, Map 1640A, scale 1:100,000.

1008   Vörösmarty, C.J., P. Green, J. Salisbury, and R.B. Lammers. 2000. Global water
1009   resources: vulnerability from climate change and population growth. *Science*
1010   289(5477): 284-288.

1011   Wassenaar, L.I., P. Athanasopoulos, and M.J. Hendry. 2011. Isotope hydrology of
1012   precipitation, surface and ground waters in the Okanagan Valley, British Columbia,
1013   Canada. *Journal of Hydrology* 411(1–2): 37-48.

1014   WHO   (World   Health   Organisation).   2017.   *Drinking   water*.
1015   http://www.who.int/mediacentre/factsheets/fs391/en/ (updated July 2017).

1016   Wolfe, B.B., T.L. Karst-Riddoch, R.I. Hall, T.W. Edwards, M.C. English, R. Palmini, S.
1017   McGowan, P.R. Leavitt, and S.R. Vardy. 2007. Classification of hydrological
1018   regimes of northern floodplain basins (Peace–Athabasca Delta, Canada) from
1019   analysis of stable isotopes (δ18O, δ2H) and water chemistry. *Hydrological*
1020   *Processes* 21(2): 151-168.

1021   World Water Assessment Programme (WWAP). 2009. *The United Nations World Water*
1022   *Development Report 3* : w*ater in a changing world*. Paris: UNESCO.

1023   Yi, Y., J.J. Gibson, J.-F. Hélie, and T.A. Dick. 2010. Synoptic and time-series stable
1024   isotope surveys of the Mackenzie River from Great Slave Lake to the Arctic Ocean,
1025   2003 to 2006. *Journal of Hydrology* 383(3): 223-232.

Domains	Hydrological components	Geological units	Hydrogeological units and aquifers
Atmosphere	(1) Precipitation (rain & snow)	-	-
Surface	(2) Snowpack (3) Surface water (4) Spring	-	-
Subsurface (groundwater)		C1 Eskers & moraines E Surface sediments near eskers	(5) Unconfined granular aquifer
		D Glaciolacustrine clay & silt	Regional aquitard
		C2 Sediments underlying clay	(6) Confined granular aquifer
		B Till	-
		A Fractured rock	(7) Unconfined or (8) confined fractured rock aquifer

Type of samples	Number of samples (n)	Sampling timeline
Precipitation	164	Monthly samples at four stations 2009-2015
Snowpack	31	March 2014 (n=31)
Springs	76	Summer 2009 (n=30) Summer-Autumn 2010 (n=41) Summer-Autumn 2013 (n=5)
Kettle lakes	14	Summer 2009 (n=14)
Surface waters	85	Summer-Autumn 2013 (n=85)
Confined fractured rock aquifer	105	Summer-Autumn 2006 (n=14) Summer-Autumn 2010 (n=26) Summer 2013 (n=65)
Unconfined fractured rock aquifers	38	Autumn 2006 (n=2) Summer 2010 (n=7) Summer-Autumn 2013 (n=29)
Confined granular aquifers	53	Summer-Autumn 2006 (n=2) Summer-Autumn 2010 (n=15) Summer 2013 (n=36)
Unconfined granular aquifers	79	Summer-Autumn 2006 (n=2) Summer 2009 (n=14) Summer-Autumn 2010 (n=25) Autumn 2011 (n=15) Summer-Autumn 2013 (n=23)
Total	645	2006-2015

Surface waters	Names	Sampling techniques	Dates
Kettle lakes	-	1 m from the lake shore / Telescopic pole / 0.5-1.5 m below surface	Summer 2009
Fault Lakes	Opasatica		Summer 2013
	Rémigny		
	Témiscamingue	Boat / Telescopic pole / 0.5-1.5 m below surface	
	Tee	Boat / Plastic tubing equipped with an inertial valve / 0.5-1.5 m below surface	Autumn 2013
Lakes on clay	Macamic	Sampling at the outlet of the lake / Telescopic pole / 0.5-1.5 m below surface	Summer 2013
	Abitibi		
Rivers	Outaouais	Boat / Telescopic pole / central part of the main channel / 0.5-1.5 m below surface	
	Duparquet	Sampling near the central part of the main channel / Telescopic pole or Bailer / 0.5-1.5 m below surface	
	La Sarre		
	From lac Mance		
	Between Beauchastel and Montbeillard lakes		
	Between Routier and Vallet lakes		
	Between Rondelet and Des Quinze lakes		
	Between two lakes (Mont Brun sector)		
Small streams	-	Sampling near the central part of the main channel / Telescopic pole or Bailer / 0.5-1.5 m below surface	Summer/Autumn 2013

In situ parameters	Stability criteria
Temperature (°C)	± 0.1
pH (pH unit)	± 0.1
Specific electrical conductivity (μS/cm)	± 2%
Dissolved oxygen (mg/L)	± 0.2
Redox potential (mV)	± 10
Turbidity (visual observation)	Constant color/opacity

Stations	n	δ^2H (‰ VSMOW)	$\delta^{18}O$ (‰ VSMOW)
Station 1 (Béarn)	24	-91.9	-13.0
Station 2 (Montbeillard)	13	NA	NA
Station 3 (Sainte-Hélène-de-Mancebourg)	24	-100.9	-14.2
Station 4 (Amos)	24	-84.5	-12.0

Refer to Figure 1 for stations locations; n: number of samples.

NA: averages values are not provided owing to a lack of data from November to April.
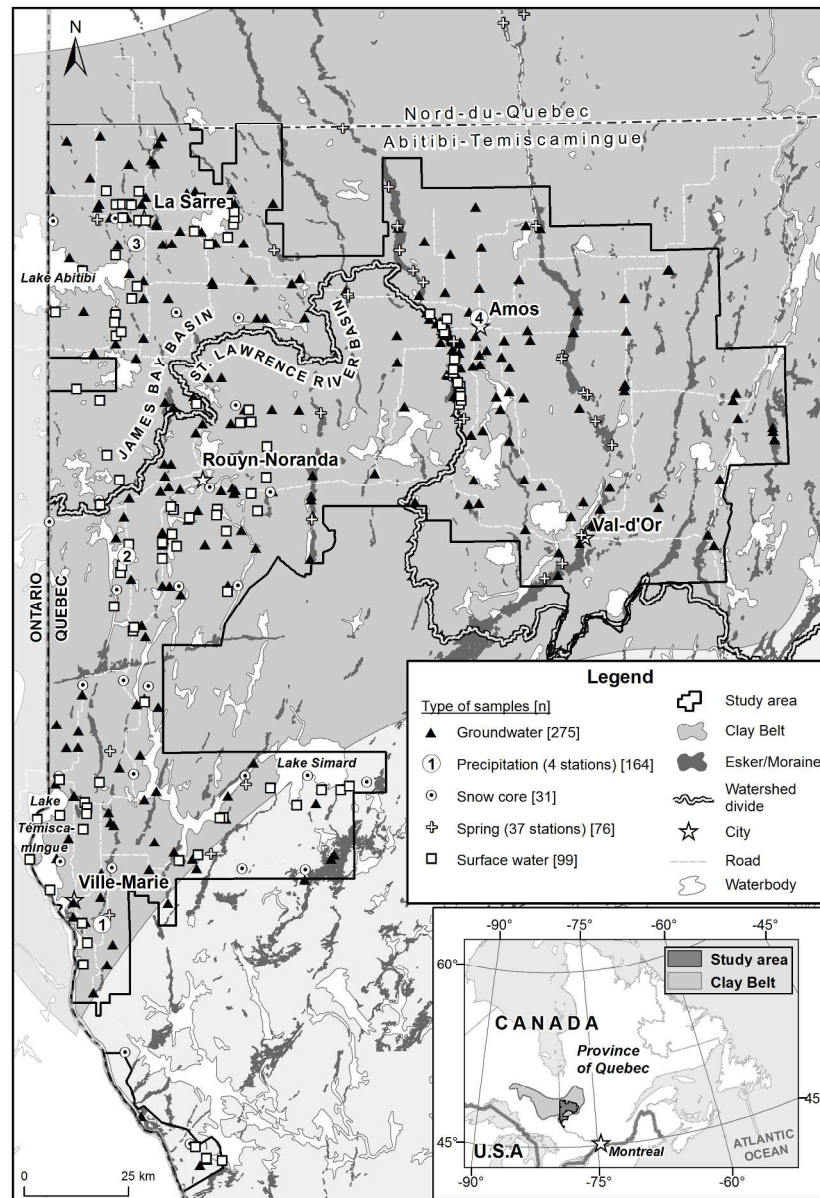
Figure 1. Study area with the location of sampling sites. The number (n) of available samples is shown brackets in the legend. The limits of the study area correspond to that of previous studies from Cloutier et al. (2013; 2015). The continental water divide between the St. Lawrence and the James Bay basins is also shown.

190x270mm (300 x 300 DPI)
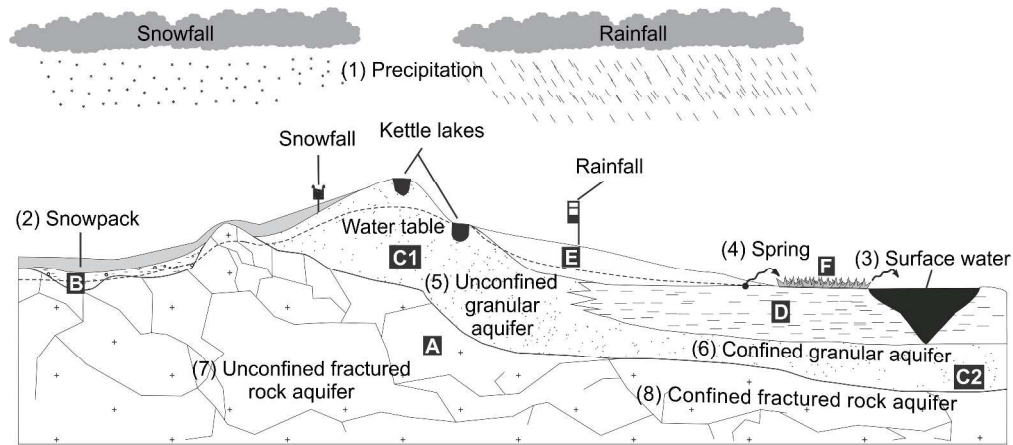
Figure 2. Regional hydrogeological conceptual model and water sampling scheme used to characterize the isotopic signature of all hydrological system components. (A) Fractured bedrock; (B) Till; (C1) Eskers and moraines; (C2) glaciofluvial sediments found between eskers and moraines, under the clay plain; (D) fine grained deep-water glaciolacustrine sediments; (E) Sublittoral sands and beach or eolian sediments; (F) Organic deposits. The numbers (1 to 8) correspond to the sampled hydrological components and hydrogeological units, as identified in table 1.

417x182mm (300 x 300 DPI)
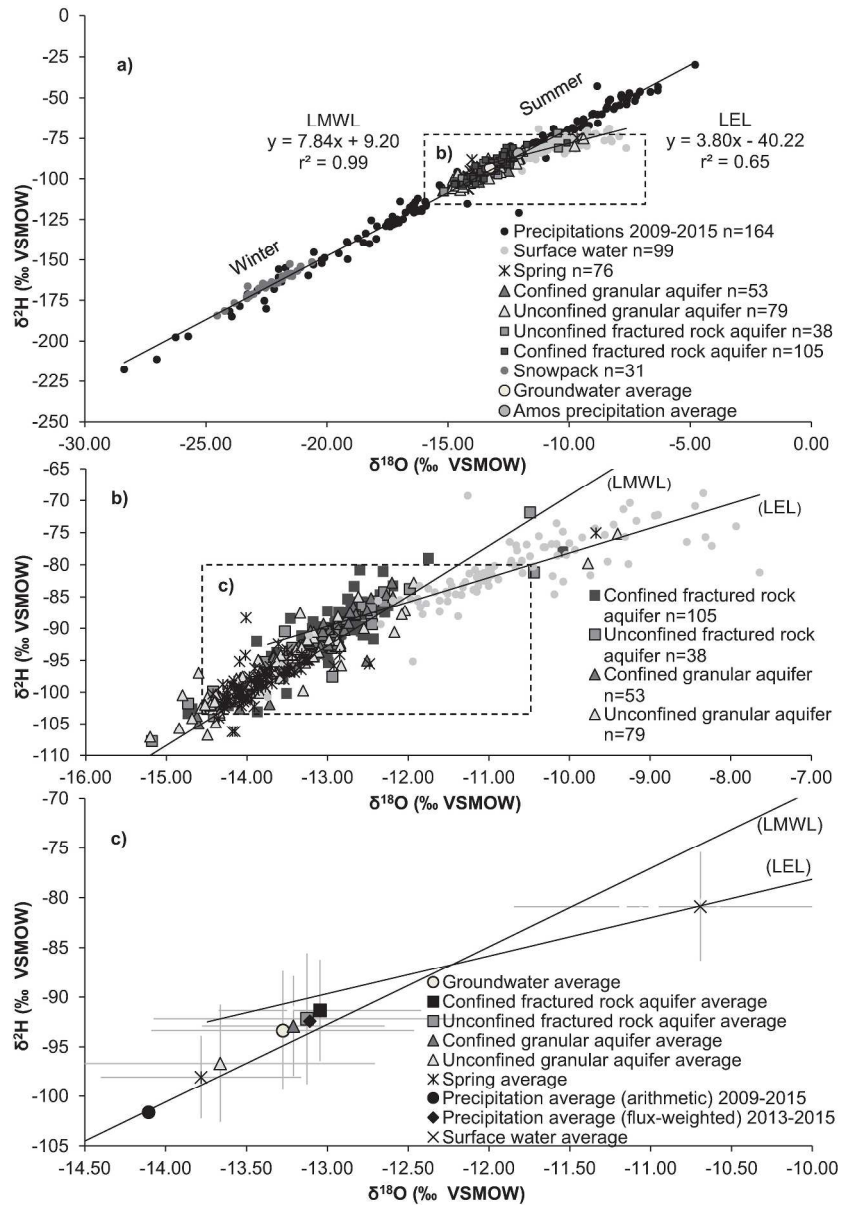
Figure 3. Isotopic composition of precipitation, surface waters, springs and groundwater. All data are shown in (a) whereas figure (b) provides a zoom on the surface and groundwater data. Average values are provided in figure (c). The flux-weighted average for precipitation is based on the three stations (Sainte-Hélène-de-Mancebourg, Amos, Bearn) where precipitation samples were collected between 2013-2015. The value correspond to the mean of the flux-weighted averages calculated for each station. The arithmetic average calculated for all precipitation samples is also shown. The error bars in (c) correspond to the standard deviation calculated for each sample series. The local meteoric water line (LMWL) and local evaporation line (LEL) derived from the data are also shown.

275x397mm (300 x 300 DPI)
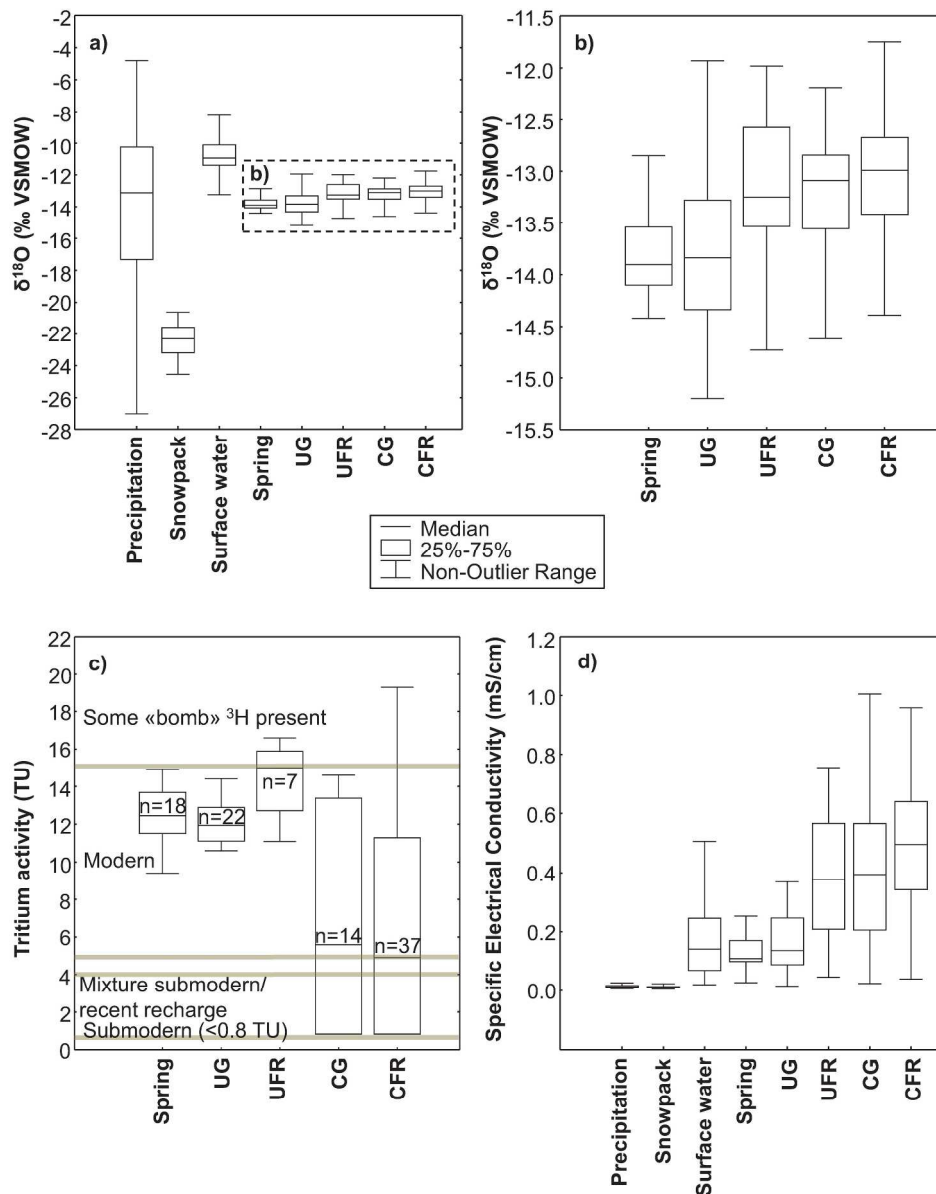
Figure 4. $\delta^{18}O$ (a; b), ^3H (c) and SEC (d) boxplots for precipitation, surface waters, springs and groundwater. Outlier data are excluded; the non-outlier range is defined as maximum and minimum values within 1.5 times the interquartile range. The available $\delta^{18}O$ data are shown in (a) whereas a clearer view of surface and groundwater data is provided in (b). The classification reported in (c) is adapted from Clark and Fritz (1997). UG: unconfined granular aquifers; UFR: unconfined fractured rock aquifers; CG: confined granular aquifers; CFR: confined fractured rock aquifers; SEC: specific electrical conductivity. In (a) and (d), the samples collected from the snowpack and at the precipitation monitoring stations are shown separately.
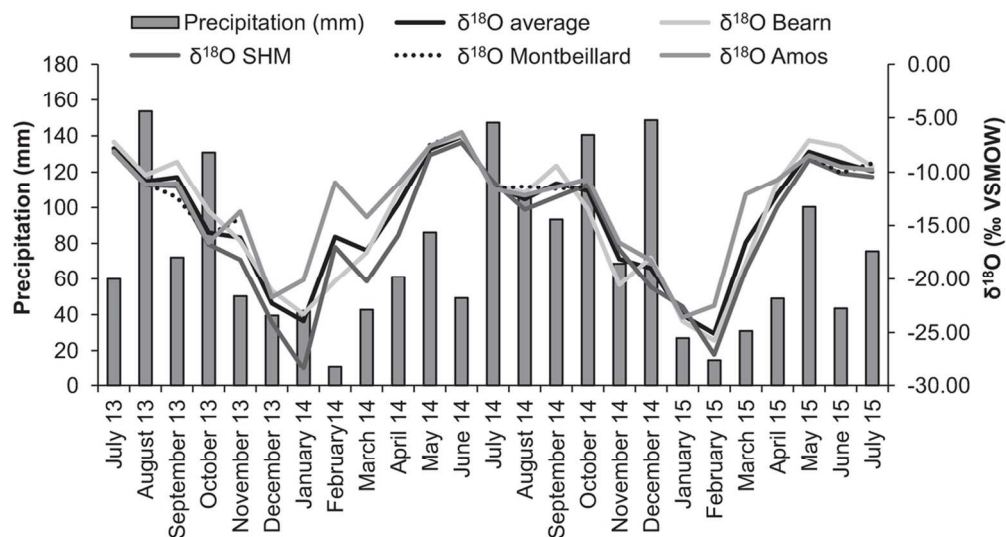
239x301mm (300 x 300 DPI)

Figure 5. Seasonal variations in precipitation amounts and $\delta^{18}O$ composition. See figure 1 for the location of monitoring stations. The histogram showing precipitation amounts is based on data from July 2013 to July 2015 as recorded at the monitoring stations. SHM: Sainte-Hélène-de-Mancebourg.
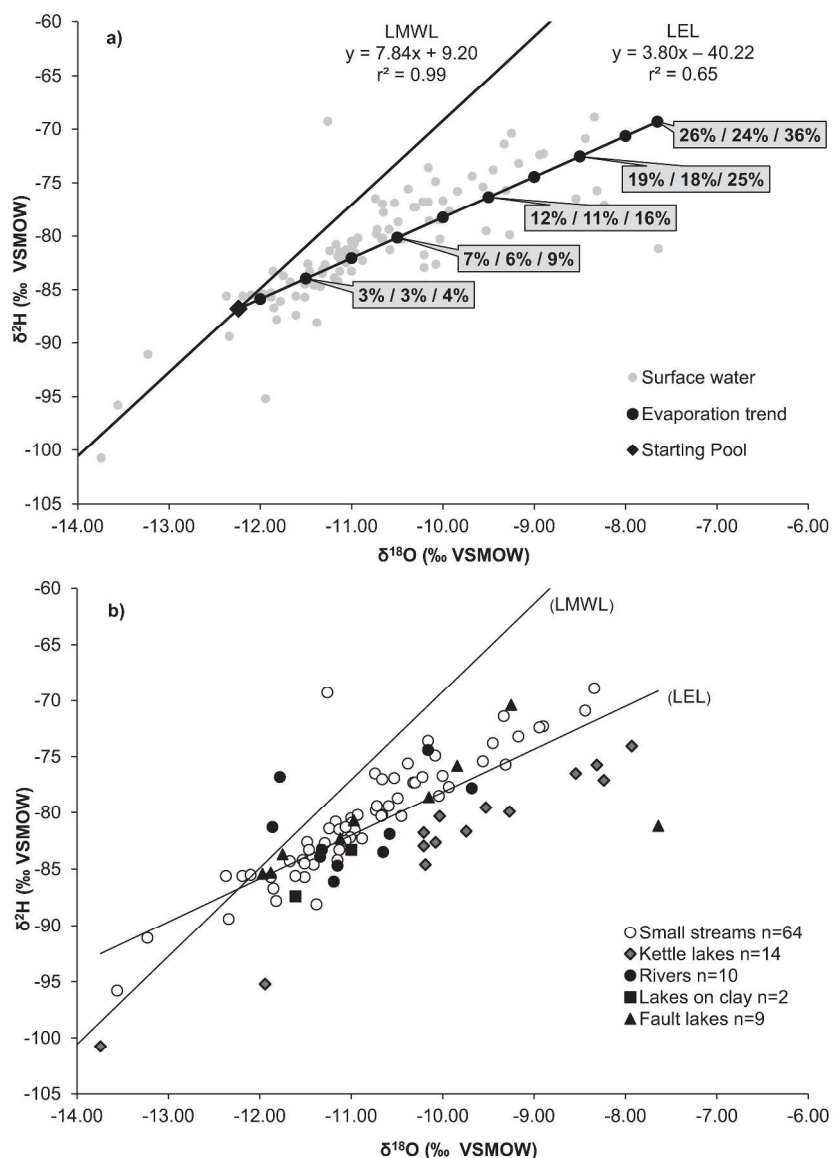
104x57mm (300 x 300 DPI)

Figure 6. Interpretation of the isotopic compositions of surface waters. Data in (a) represent the local evaporation line evaluated using the 99 available surface water samples. The E/I ratios are shown for points plotting on the LEL at 0.5‰ intervals along the x-axis. These E/I ratios are shown for three scenarios (see text for details). Further details with respect to the types of surface water samples are provided in (b) and in table 3.
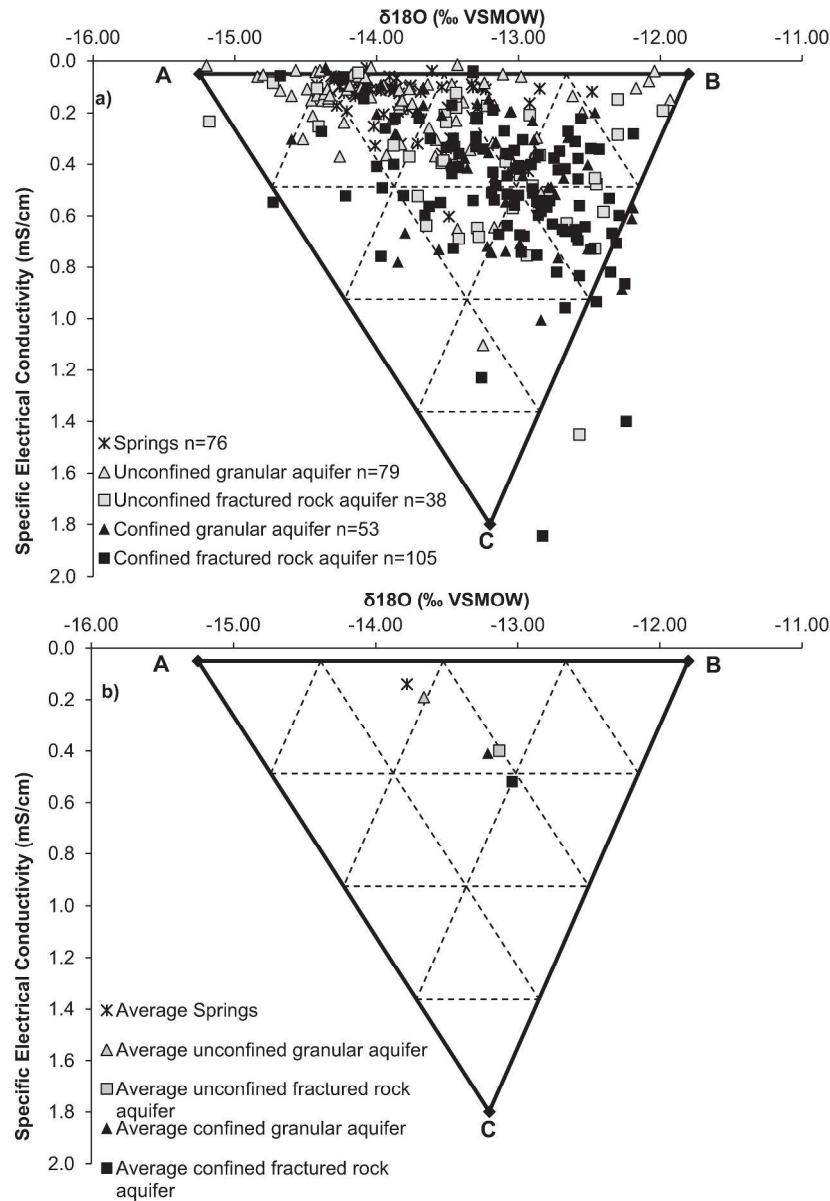
275x397mm (300 x 300 DPI)

Figure 7. Specific electrical conductivity (SEC) vs $\delta^{18}O$ of springs, surface waters and groundwater. Three end-members are shown: «A» corresponds to groundwater recharged during snowmelt, «B» corresponds to groundwater that is less impacted by snowmelt induced recharge and «C» corresponds to geochemically evolved groundwater found further along regional flowpaths. See text for further details. The six main outliers (as described in the text) are not shown in this figure. Figure (a) shows the distribution of data whereas the corresponding averages are shown in (b).
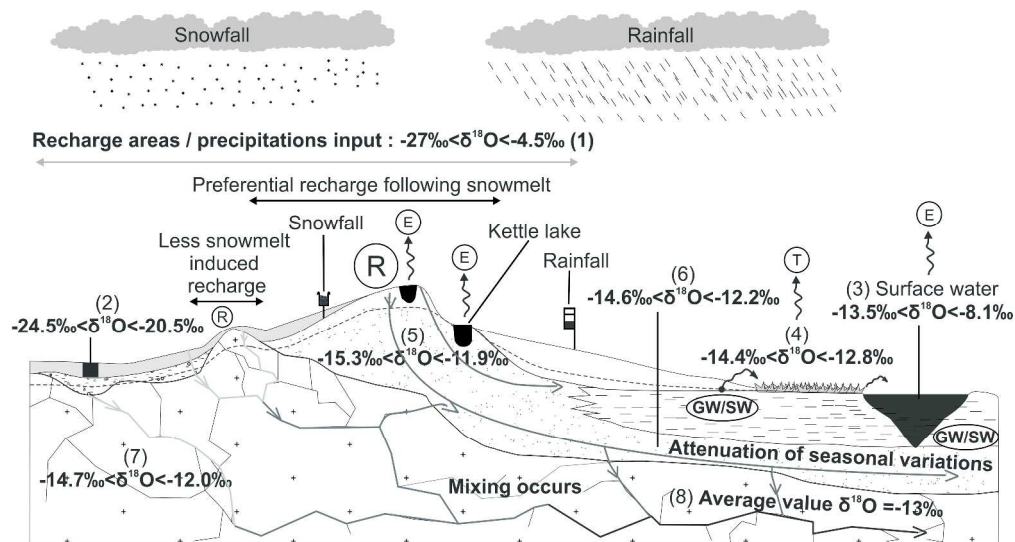
263x365mm (300 x 300 DPI)

Figure 8. Isotopic variations within local, intermediate and regional flow systems. The range of measured isotopic compositions is shown for the sampled hydrological components and hydrogeological units, as identified in tables 1 and 2. Areas of preferential snowmelt induced recharge are identified. Flowpaths at various scales are shown. (R) Recharge area; (E) Evaporation; (T) Transpiration; (GW/SW) Groundwater / surface water interactions (herein mainly groundwater exfiltration). The numbers (1 to 8) correspond to the sampled hydrological components and hydrogeological units, as identified in table 1.

423x226mm (300 x 300 DPI)